ICP/EXT-03-00088

Spatial Distribution of Neptunium and Uranium Partition Coefficients (K_d) for Interbed Sediments at a Radioactive Waste Subsurface Disposal Area

Molly K. Leecaster
Larry C. Hull

Idaho Completion Project

Bechtel BWXT Idaho, LLC

February 2004

ICP/EXT-03-00088
Revision 0
Project No. 23378

Spatial Distribution of Neptunium and Uranium Partition Coefficients (K_d) for Interbed Sediments at a Radioactive Waste Subsurface Disposal Area

Molly K. Leecaster
Larry C. Hull

February 2004

Idaho Completion Project
Idaho Falls, Idaho 83415

Prepared for the
U.S. Department of Energy
Assistant Secretary for Environmental Management
Under DOE/NE Idaho Operations Office
Contract DE-AC07-99ID13727

ABSTRACT

Computer simulations of the uranium and neptunium transport from the buried waste at the Idaho National Engineering and Environmental Laboratory radioactive waste subsurface disposal area predict that uranium and neptunium will exceed risk-based concentrations in the aquifer if no remedial actions are implemented. The simulations involve predicting the migration of the radionuclides through a 180 m thick vadose zone consisting of alternating layers of sediment and basalt. Basalt is not considered to provide retardation for the movement of uranium and neptunium, but the sediments are believed to significantly retard the migration of radionuclides. Samples were collected from two sedimentary interbeds at 12 locations within the burial ground and analyzed for clay mineralogy, grain size, surface area, cation exchange capacity, and extractable oxides. Distribution coefficients (K_d) for neptunium and uranium were measured on 36 sediment samples in a synthetic ground water. K_d values for neptunium ranged from 0.1 to 251 mL/g with a median of 35.0 mL/g. K_d values for uranium ranged from 0.6 to 48 mL/g with a median of 17.9 mL/g. Median K_d values for both neptunium and uranium are higher than values used in previous risk assessments. No statistically significant difference in neptunium K_d values was found between the interbeds, but significant differences were found for uranium K_d, with the deeper C-D interbed having slightly lower K_d values than the shallower B-C interbed for paired measurements. From correlations between measured K_d values and material properties, sorption of uranium and neptunium is primarily related to cation exchange capacity, extractable iron, and the prevalence of clay minerals. Various parametric models for predicting K_d values from material properties were evaluated, but did not provide an efficient and accurate means of predicting K_d from material property measurements. Little spatial correlation was found for either radionuclide in either interbed based on the limited number of samples collected for this investigation. Spatially distributed values were generated, but with the limited number of sampling points, they did not provide a significant improvement over the current approach of using constant parameter values for all elements of the spatial domain.

CONTENTS

FIGURES

TABLES

ACRONYMS

ANOVA	analysis of variance
ASTM	American Society for Testing and Materials
CERCLA	Comprehensive Environmental Response, Compensation, and Liability Act
CV	coefficient of variance
DOE	Department of Energy
INEEL	Idaho National Engineering and Environmental Laboratory
MSE	mean square error
RWMC	Radioactive Waste Management Complex
SDA	Subsurface Disposal Area
TSA	Transuranice Storage Area

Spatial Distribution of Neptunium and Uranium Partition Coefficients (K_d) for Interbed Sediments at a Radioactive Waste Subsurface Disposal Area

1. INTRODUCTION

Past U.S. Department of Energy (DOE) activities associated with the production of nuclear weapons, fuel reprocessing, and research into the peaceful uses of the atom have generated low-level and transuranic radioactive waste. The Radioactive Waste Management Complex (RWMC) at the Idaho National Engineering and Environmental Laboratory (INEEL) (see Figure 1) has been used since 1952 for subsurface disposal and above ground storage of radioactive waste. Low-level waste is buried in shallow (i.e., depth < 7.6 m) pits and trenches in the Subsurface Disposal Area (SDA). Prior to 1970, waste containing transuranic elements was also buried in pits and trenches. Transuranic waste received since 1970 has been stored above ground in the Transuranic Storage Area (TSA). Contact-handled transuranic waste stored in the TSA is being shipped to the Waste Isolation Pilot Plant in New Mexico for permanent disposal. The fate of the buried waste will be decided through the Comprehensive Environmental Response, Compensation, and Liability Act (CERCLA) process.

Almost 350 t of uranium are estimated to have been buried in the SDA since the early 1950s (Holdren et al. 2002). Most of the uranium is in the form of depleted uranium; however, enriched uranium is also present in waste generated from reprocessing highly enriched spent nuclear fuel. The current estimated inventory of Np-237 in the SDA is small, but alpha decay of Am-241 will increase the Np-237 inventory over time. Predictions of uranium and neptunium migration at the SDA have been made for a performance assessment to comply with DOE orders (Case et al. 2000; McCarthy et al. 2000) and to support CERCLA risk assessment (Magnuson and Sondrup 1998; Holdren et al. 2002). Risk assessment calculations show that Np-237 and uranium isotopes, through the groundwater ingestion pathway, pose peak risks in excess of 1×10^{-4} from buried waste if no remedial action is taken (Holdren et al. 2002). In all of these simulation studies, transport was modeled using a linear, reversible partition coefficient (K_d) derived from laboratory measurement of K_d on a composite sedimentary interbed sample (Newman et al. 1996).

A computer simulation model for transport of dissolved-phase contaminants through the vadose zone at the SDA was originally developed by Magnuson and Sondrup (1998) and was updated and improved in 2002 (Holdren et al. 2002). The model treats the subsurface at the SDA as a heterogeneous, anisotropic, and porous medium. The vadose zone is divided into layers consisting of sediment or fractured basalt (see Figure 2). Sediment layers are simulated as a porous medium of variable thickness. The hydraulic properties used in the computer model vary spatially based on a kriging analysis of point measurements (Leecaster 2002). In contrast to the hydrologic properties, constant K_d values of 6 mL/g for uranium and 8 mL/g for neptunium are assumed to apply to all sediments at the SDA. Transport in the basalt layers is assumed to take place only through fractures, with no exchange of water or solutes between fractures and the basalt matrix. This is accomplished by treating the basalt as a low-porosity, high-permeability, equivalent porous medium. The model assumes no sorption of radionuclides on basalts, so the K_d for all basalt layers is 0 mL/g for all radionuclides.

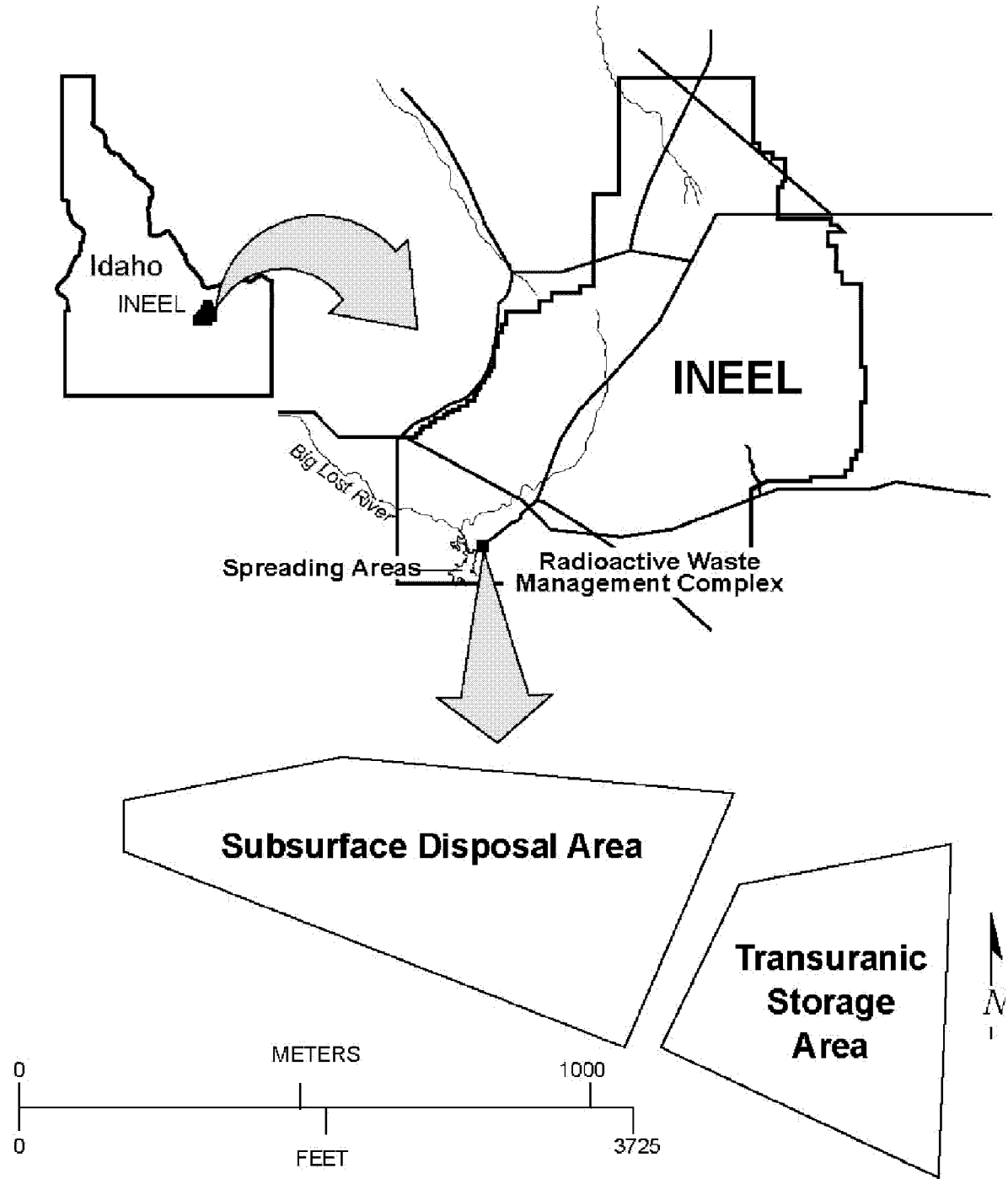

Figure 1. Map of the Idaho National Engineering and Environmental Laboratory showing the location of the Radioactive Waste Management Complex.

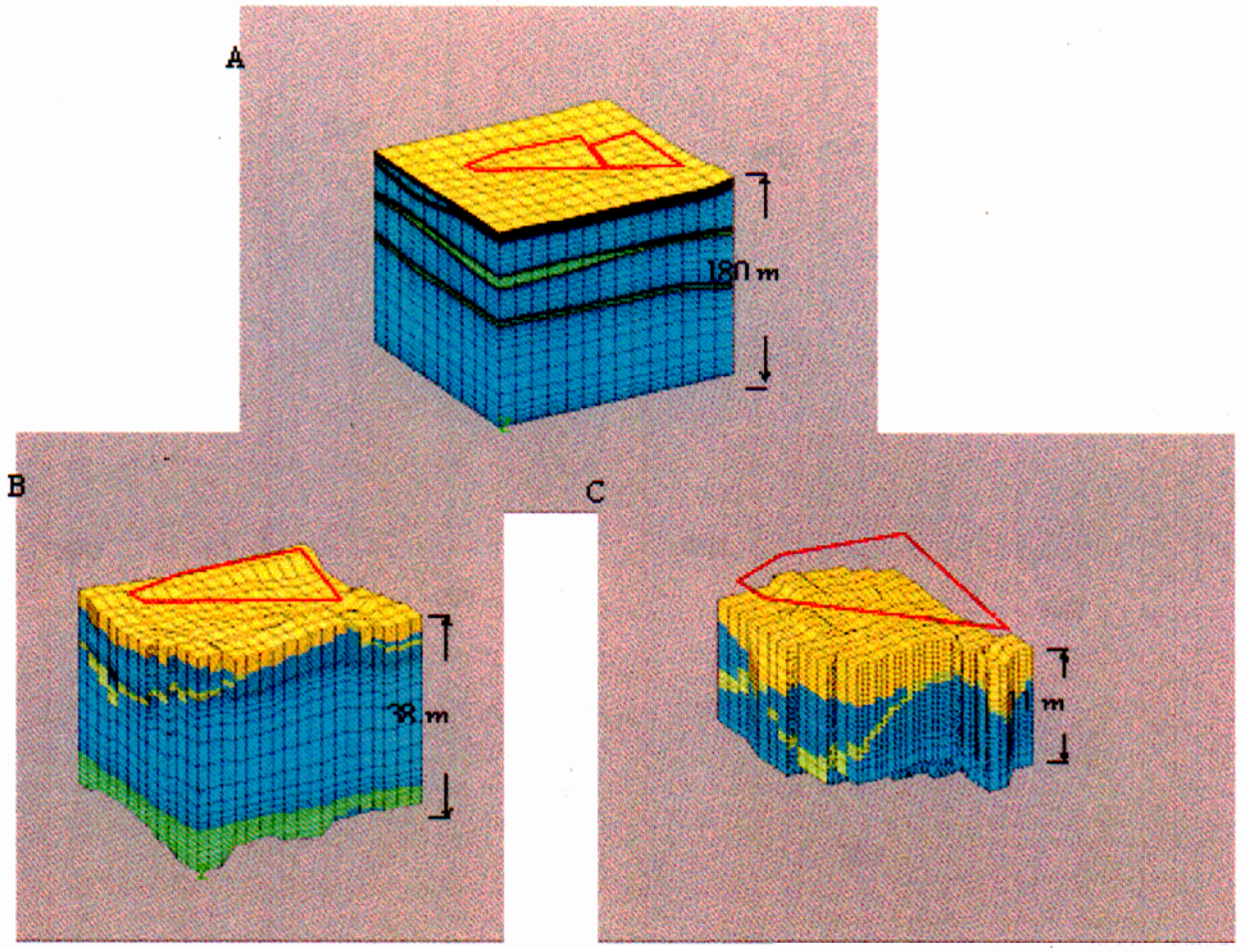

Figure 2. Conformable grid for base domain (A) and locally refined domains (B and C). Surficial sediments are shown in yellow, interbeds in green, and fractured basalt in blue.

Recognizing the need for improved defensibility of risk assessment models in support of the INEEL CERCLA remediation program, additional investigations have been conducted to measure site-specific partition coefficients for SDA sediments (Fjeld et al. 2001; Grossman et al. 2001; Ayaz et al. 2003). In this report, the spatial variability in the measured K_d values is analyzed to determine if a spatially variable parameter can provide additional refinement in transport properties for risk and performance assessment models. The goal was to investigate the spatial correlation of the K_d values to determine if the data from multiple wells would be useful for assigning block-specific values for use in fate and transport models. Three tasks were completed toward the goal. The first task was to investigate the sources of variation in the data. The second task was to investigate relationships among measured sediment properties. The third task was to spatially model the K_d values.

1.1 Background

The transport of contaminants through the subsurface depends in part on the contaminant-specific partitioning coefficient. The measure of contaminant retardation most used is the K_d. The K_d parameter describes the potential for the adsorption of dissolved contaminants in contact with sediment. As typically used in fate and contaminant transport calculations, the K_d is defined as the ratio of the contaminant

concentration associated with the solid to the contaminant concentration in the surrounding aqueous solution when the system is at equilibrium (EPA 1999).

$$K_d = \frac{C_{ads}}{C_{sol}} \quad (1)$$

where

K_d = empirical partition coefficient at equilibrium (mL/g)

C_{ads} = concentration of parameter on the solid (mg/g, Bq/g, mole/g)

C_{sol} = concentration of parameter in solution (mg/mL, Bq/mL, mole/mL)

Site-specific K_d values should be used for site-specific contaminant and performance assessment calculations (EPA 1999). Key assumptions implicit with the K_d construct are all adsorption sites are accessible, all sites adsorb the contaminant equally, and the number of adsorption sites exceeds the maximum expected contaminant concentration. Ideally, site-specific K_d values should be measured for the range of aqueous and geological conditions in the system to be modeled. This is especially limiting for groundwater contaminant models because it requires that K_d values should be used only to predict transport in systems chemically identical to those used in the laboratory measurement of the K_d. Variation in either sediment or aqueous chemistry of the system can result in extremely large differences in K_d values. Commonly, literature-derived K_d values are used for screening calculations without regard to differences in site-specific conditions.

Hydrologic models are important tools for predicting the movement of groundwater and the constituents carried therein. Understanding flow and transport processes is especially important for areas like the SDA where hazardous constituents may be in the groundwater. To apply deterministic hydrologic models, the region of interest is divided into cells or nodes. Each block requires values of hydrogeologic and transport properties, so that many characteristics need to be known at a small scale over the entire area of interest. These variables are measured only at a sample of sites; therefore, a method to extrapolate from the sample sites to the entire domain of interest is needed. Contaminant transport models require a value of K_d for each constituent of interest assigned at the grid block. A common approach used for screening, or where no site-specific K_d values are available, is to assign a single parameter value for K_d to all locations in the model.

One alternative to a single, site-wide K_d assignment is to use a parametric-K_d model (EPA 1999). This model varies the K_d value according to the chemistry and mineralogy of the system at the node being modeled (MacIntyre et al. 1998; Painter et al. 2001). The presence of correlation between K_d and material properties does not imply causation and does not necessarily provide information on the mechanism. The added complexity in solving the transport equation with the parametric-K_d sorption model and its empirical nature may be the reasons this approach has been used sparingly.

Another alternative to a single, site-wide K_d assignment is to use mechanistic models to explicitly accommodate for the dependency of K_d values on contaminant concentration, charge, competing ion concentration, variable surface charge on the sediment, and solution species distribution (Davis and Kent 1990; Turner 1995; Turner and Pabalan 1999). This is desirable but rarely applied. Natural mineral surfaces are very irregular and difficult to characterize, thus difficult to model.

Yet another alternative to a single, site-wide K_d assignment is to use the K_d values available at a sample of locations across the site to spatially model K_d values at all nodes being modeled. The K_d values

are predicted at nodes based on spatial correlation structure rather than correlation to other values or mechanistic models or knowledge of the mechanism. A study of strontium K_d found spatial correlation in horizontal as well as vertical profiles (Robin et al. 1991) in alluvial sands in the Borden aquifer. Viswanathan et al. (2003) found that spatially varying sorption characteristics affected the predicted transport at Yucca Mountain.

1.2 Setting

The INEEL is located on the eastern Snake River Plain, a northeast trending structural basin about 320 km long and 80 to 110 km wide in southeastern Idaho (see Figure 1). The plain is underlain by a layered sequence of tertiary and quaternary volcanic rocks and sedimentary deposits (Anderson and Lewis 1989). Volcanic rocks in this sequence consist of basaltic lava flows and cinder beds. During periods of volcanic quiescence, fluvial, lacustrine, and eolian sediments were deposited. Alternating periods of volcanic activity and sedimentary deposition have accumulated into a complex sequence of layers (see Figure 3). The water table is at a depth of about 180 m in the vicinity of the SDA.

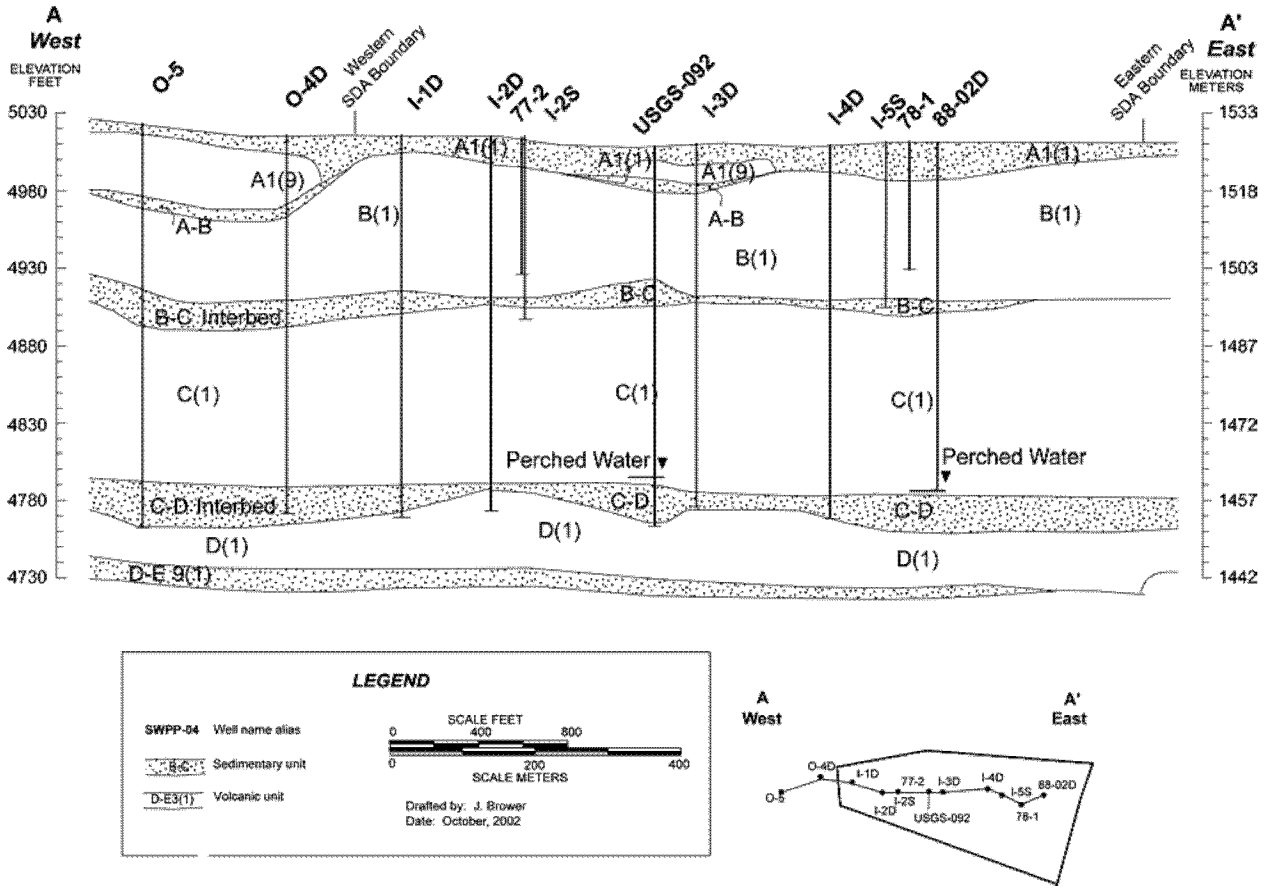

Figure 3. Geologic cross section of the Subsurface Disposal Area showing the interlayering of basalt and sediment.

There are a number of important sedimentary units beneath the SDA that are considered to be crucial barriers to downward migration of radionuclides from buried waste (Magnuson and Sondrup 1998; McCarthy et al. 2000). The ability of these sedimentary interbeds to retard the migration of contaminants is the focus of characterization efforts. The fractured basalt units are not considered to

provide significant retardation; therefore, the units are of secondary interest at this time. The shallowest interbed is the A-B interbed (between basalt flows A and B) that is mainly found in the northern and western parts of the SDA. The depth to the top of the A-B interbed is between 5.5 and 16.8 m below land surface. The B-C interbed ranges in depth from 26.5 to 40 m with thickness ranging from 0 to 12.2 m and averaging 4 m. The C-D interbed ranges in depth from 66.5 to 77.1 m. The C-D interbed thickness ranges from 1.5 to 9.8 m and averages 5.2 m.

The sedimentary interbeds have a nominal mineralogy of 35% quartz, 30% feldspar, 4% calcite, 10% pyroxene, 2% dolomite, and 19% clays (Bartholomay et al. 1989; Bartholomay 1990). Predominant clay minerals are illite, smectite, and kaolinite. The mineralogy of sediments at the SDA correlates with the mineralogy of source areas in the adjacent mountain ranges. Sediments in different interbeds are mineralogically very similar, reflecting a fairly uniform source area and depositional process over time (Bartholomay 1990).

2. EXPERIMENTAL AND DATA ANALYSIS METHODS

A series of twelve vadose zone wells was drilled in and around the SDA in 1999 to install moisture-monitoring equipment in the SDA and to collect samples to measure material properties of the sedimentary interbeds for parameterization of computer models (see Figure 4). Samples were collected from the B-C and C-D sedimentary interbeds for hydrologic and geochemical characterization. Samples for K_d measurements are grab samples collected from individual layers within the B-C and C-D interbeds. Samples were selected from available core material, based on visual interpretation to represent a range of color and grain size characteristics. Uranium and neptunium K_d values were measured in 36 samples collected from two to four depths at twelve surface locations. Twenty samples from nine locations were taken within the B-C sediment interbed and sixteen samples from ten locations were taken from the C-D sediment interbed.

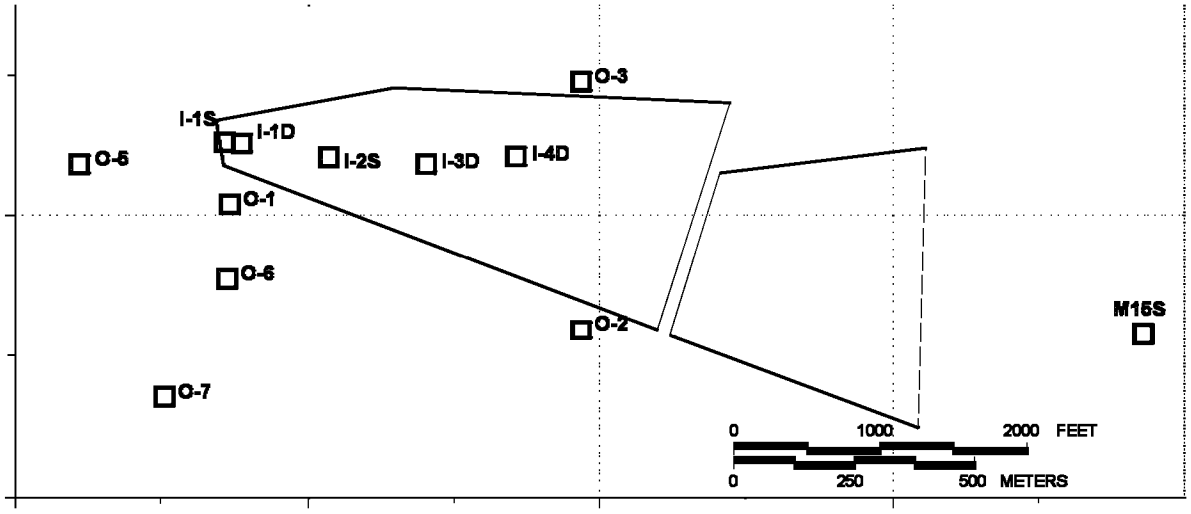

Figure 4. Map of the Subsurface Disposal Area showing the wells where samples have been collected for measuring uranium and neptunium adsorption isotherms.

2.1 Material Characterization

Geochemical properties, measured in this study, relevant to sorption, are clay mineralogy, surface area, cation exchange capacity, exchangeable cations, and extractable oxides of aluminum, iron, manganese, and silicon. Grain size analyses (see Table 1) were performed by sieving the size fraction greater than a #200 U.S. standard sieve (i.e., 0.074 mm) and differentiating silt and clay sized material using an hydrometer (ASTM 1963). Size fractions were separated at 2 mm for gravel and sand, 0.074 mm for sand and silt, and 0.004 mm for silt and clay. Clay mineralogy (see Table 1) was determined by x–ray diffraction on the clay-size fraction (Whittig and Allardice 1986). Surface area of the material (see Table 2) was determined by multipoint nitrogen absorption using Brunauer-Emmett-Teller surface area analysis (Brunauer et al. 1938). Cation exchange capacity and exchangeable cations were determined separately (see Table 2). Cation exchange capacity was measured by sodium saturation followed by extraction with ammonium acetate (Rhoades 1982). Exchangeable cations were determined by ammonium acetate extraction, with the difference that the sodium saturation step was bypassed. The collected extract was analyzed for calcium, magnesium, strontium, sodium, and potassium by inductively coupled plasma emission spectrometry. When measuring the cation exchange capacity, soluble salts in the sample are dissolved during the sodium saturation step, and do not contribute to the measured cation exchange capacity. When the sodium saturation step is skipped, the soluble salts dissolve into the solution used to determine the exchangeable cations. The sum of exchangeable cations is expected to be larger than the measured cation exchange capacity because of the soluble salt contribution. Extractable oxides (see Table 3) were determined by the citrate–bicarbonate–dithionite method (Jackson et al. 1986). Extracts were analyzed for aluminum, iron, manganese, and silicon by inductively coupled plasma emission spectrometry.

2.2 Batch Isotherm Experiments

Uranium and neptunium sorption isotherms were measured on 36 sediment samples collected from sedimentary interbeds underlying the INEEL SDA. Sediment material used for sorption experiments was sieved through a 2-mm sieve to remove gravel-sized material as recommended by EPA (EPA 1999). In calculating final K_d values for use in the spatial distribution analysis, the measured K_d values were adjusted for the gravel-size weight fraction by assuming the sorption to the gravel would be zero. This assumption has been shown to be reasonable for coarse-grained sediments (Mattigod and Martin 2001). Reported K_d values are representative of the material as removed from the cores. Following sieving, sediment samples were pretreated with a groundwater simulant, according to American Society for Testing and Materials (ASTM) D 4319–93 (ASTM 1993), in four contact intervals: three of 15 minutes and one of 24 hours. After each contact interval, the sediment was centrifuged at 1,000 g for 5 minutes and decanted. The aqueous solution for the experiments was a simulated groundwater, prepared by adding reagent grade chemicals to distilled, deionized water. The simulated groundwater contains important cations and anions present in vadose zone waters at the SDA (see Table 4). Sediment suspensions were prepared by adding a weighed amount of sediment to groundwater simulant to produce suspended solids concentrations between 50,000 and 100,000 mg/L.

Stock uranium or neptunium spike solution was prepared using U-233 or Np-237 at high activity in acidic water. Test solutions were then prepared by adding a small volume of the spike solution to the test solution/sediment suspension to achieve the desired final concentration in the test solution. The pH of the test solution was then adjusted to a value of 8.0 ± 0.2 using hydrochloric acid or sodium hydroxide. Each isotherm was determined by duplicate equilibrations at each of five initial radionuclide concentrations (see Table 5). Batch sorption experiments were carried out for time periods between 48 and 56 days, with the length of the tests based on results from a preliminary kinetic adsorption study (Grossman et al. 2001).

Table 1. Material analysis results, grain size analysis, and quantitative clay mineralogy.

Well ID	Well Alias	Sample ID	Interval Top (m bls)	Interval Bottom (m bls)	Interbed	Clay Fraction (g/g sed)	Silt Fraction (g/g sed)	Sand Fraction (g/g sed)	Gravel Fraction (g/g sed)	Smectite Fraction (g/g clay)	Illite Fraction (g/g clay)	Kaolinite Fraction (g/g clay)	Smectite (g/g sed)	Illite (g/g sed)	Kaolinite (g/g sed)
MON-A-009	M15S	7DS09501	41.5	41.9	B-C	0.069	0.157	0.636	0.138	0.48	0.24	0.28	0.033	0.017	0.019
MON-A-009	M15S	7DS09601	44.1	44.4	B-C	0.162	0.758	0.08	0	0.61	0.18	0.21	0.099	0.029	0.034
MON-A-009	M15S	7DS09701	69.8	70.1	C-D	0.001	0.35	0.649	0	0.19	0.81	0	<0.001	0.001	<0.001
SCI-V-011	O-01	7DS03101	31.7	31.9	B-C	0.018	0.092	0.432	0.458	0.78	0.09	0.13	0.014	0.002	0.002
SCI-V-011	O-01	7DS03301	33.5	33.8	B-C	0.451	0.53	0.018	0.001	0.7	0.11	0.19	0.316	0.05	0.086
SCI-V-011	O-01	7DS03501	71.6	71.8	C-D	0.001	0.512	0.481	0.006	0.38	0.41	0.21	<0.001	<0.001	<0.001
SCI-V-012	O-02	7DS03701	33.8	34.0	B-C	0.031	0.07	0.876	0.023	0.55	0.29	0.16	0.017	0.009	0.005
SCI-V-012	O-02	7DS03901	37.7	37.8	B-C	0.067	0.395	0.244	0.294	0.72	0.1	0.18	0.048	0.007	0.012
SCI-V-012	O-02	7DS08201	74.1	74.4	C-D	0.064	0.81	0.126	0	0.54	0.3	0.16	0.035	0.019	0.01
SCI-V-013	O-03	7DS04301	29.7	29.9	B-C	0.037	0.156	0.596	0.211	0.67	0.1	0.23	0.025	0.004	0.008
SCI-V-013	O-03	7DS04702	70.1	70.3	C-D	—	—	—	—	0.48	0.31	0.21	—	—	—
SCI-V-013	O-03	7DS04701	71.4	71.6	C-D	0.049	0.659	0.282	0.01	0.46	0.54	0	0.022	0.026	<0.001
SCI-V-014	O-06	7DS08801	32.9	33.2	B-C	0.419	0.546	0.035	0	0.65	0.13	0.22	0.272	0.054	0.092
SCI-V-014	O-06	7DS08901	36.0	36.3	B-C	0.677	0.291	0.012	0.02	0.65	0.11	0.24	0.44	0.074	0.162
SCI-V-014	O-06	7DS09001	74.1	74.7	C-D	0.16	0.546	0.202	0.092	0.58	0.26	0.16	0.093	0.042	0.026
SCI-V-015	O-05	7DS08401	34.0	34.6	B-C	0.004	0.023	0.174	0.799	0.54	0.21	0.25	0.002	0.001	0.001
SCI-V-015	O-05	7DS08501	35.9	36.2	B-C	0.149	0.599	0.248	0.004	0.77	0.09	0.15	0.115	0.013	0.022
SCI-V-015	O-05	7DS08601	38.4	38.8	B-C	0.692	0.289	0.019	0	0.57	0.17	0.27	0.394	0.118	0.187
SCI-V-015	O-05	7DS08701	38.4	38.8	B-C	0.795	0.191	0.014	0	0.6	0.16	0.24	0.477	0.127	0.191
SCI-V-015	O-05	7DS08301	75.9	76.2	C-D	0.227	0.745	0.028	0	0.53	0.26	0.21	0.12	0.059	0.048
SCI-V-016	O-07	7DS09101	40.9	41.2	B-C	0.301	0.629	0.069	0.001	0.65	0.13	0.22	0.196	0.039	0.066
SCI-V-016	O-07	7DS09201	45.1	45.4	B-C	0.247	0.721	0.032	0	0.54	0.2	0.25	0.133	0.049	0.062
SCI-V-016	O-07	7DS09301	45.1	45.4	B-C	0.23	0.736	0.034	0	0.47	0.22	0.31	0.108	0.051	0.071
SCI-V-016	O-07	7DS09401	74.7	75.6	C-D	0.016	0.156	0.828	0	0.62	0.29	0.09	0.01	0.005	0.004
SCI-V-153	I-1S	7DS00101	31.4	31.6	B-C	0.022	0.049	0.282	0.647	0.75	0.04	0.21	0.016	0.001	0.005
SCI-V-153	I-1S	7DS00301	32.7	32.9	B-C	0.208	0.294	0.378	0.12	0.61	0.15	0.25	0.127	0.031	0.052
SCI-V-153	I-1S	I1S-109	33.2	33.4	B-C	0.001	0.26	0.695	0.045	0.69	0.14	0.16	0.001	<0.001	<0.001
SCI-V-154	I-2S	7DS00701	31.4	31.6	B-C	0.055	0.197	0.687	0.061	0.71	0.09	0.2	0.039	0.005	0.011
SCI-V-154	I-2S	I2S-105	31.9	32.0	B-C	0.005	0.25	0.745	0	0.79	0.11	0.1	0.004	0.001	0.001
SCI-V-154	I-2S	7DS00901	34.1	34.3	B-C	0.558	0.405	0.037	0	0.66	0.11	0.22	0.368	0.061	0.123
SCI-V-157	I-3D	I3D-229	69.9	70.0	C-D	0.007	0.51	0.483	0	0.45	0.38	0.17	0.003	0.003	0.001
SCI-V-157	I-3D	7DS01701	70.4	70.6	C-D	—	—	—	—	0.44	0.29	0.27	—	—	—

Table 1. (continued).

Well ID	Well Alias	Sample ID	Interval Top (m bls)	Interval Bottom (m bls)	Interbed	Clay Fraction (g/g sed)	Silt Fraction (g/g sed)	Sand Fraction (g/g sed)	Gravel Fraction (g/g sed)	Smectite Fraction (g/g clay)	Illite Fraction (g/g clay)	Kaolinite Fraction (g/g clay)	Smectite (g/g sed)	Illite (g/g sed)	Kaolinite (g/g sed)
SCI-V-159	I-4D	I4D-224	68.4	68.5	C-D	0.005	0.574	0.421	0	0.4	0.6	0	0.002	0.003	0
SCI-V-159	I-4D	7DS02301	70.1	70.3	C-D	0.53	0.454	0.016	0	0.49	0.22	0.29	0.26	0.117	0.154
SCI-V-159	I-4D	I4D-231	70.3	71.2	C-D	0.002	0.46	0.538	0	0.27	0.23	0.25	0.001	0.001	0.001
SCI-V-159	I-4D	I4D-234	71.2	71.3	C-D	—	—	—	—	0.45	0.26	0.28	—	—	—
SCI-V-160	I-1D	I1D-234	71.3	71.5	C-D	0.002	0.508	0.492	0	0.42	0.55	0.04	0.001	0.001	<0.001
SCI-V-160	I-1D	7DS00501	72.6	72.7	C-D	0.066	0.37	0.495	0.069	0.32	0.65	0.04	0.021	0.043	0.003

Table 2. Material property results, surface area, and cation exchange.

Well ID	Sample ID	Interval Top (m bls)	Interval Bottom (m bls)	Interbed	Surface Area INEEL (m^2/g)	Surface Area SWRI (m^2/g)	CEC (meq/100g)	Calc CEC (meq/100g)	Exch Ca (meq/100g)	Exch K (meq/100g)	Exch Mg (meq/100g)	Exch Na (meq/100g)	Exch Sr (meq/100g)
MON-A-009	7DS09501	41.5	41.9	B-C	14.27	14.10	13.00	10.10	5.44	0.42	3.38	0.84	0.014
MON-A-009	7DS09601	44.1	44.4	B-C	17.46	19.06	14.30	26.09	19.50	0.46	5.49	0.61	0.023
MON-A-009	7DS09701	69.8	70.1	C-D	21.80	22.11	3.28	7.55	5.27	0.34	1.82	0.10	0.018
SCI-V-011	7DS03101	31.7	31.9	B-C	44.92	40.62	32.70	35.95	25.50	0.75	9.38	0.27	0.051
SCI-V-011	7DS03301	33.5	33.8	B-C	30.41	31.27	20.00	31.72	25.10	0.65	5.70	0.23	0.038
SCI-V-011	7DS03501	71.6	71.8	C-D	37.54	39.03	19.60	22.42	15.70	0.83	5.60	0.24	0.040
SCI-V-012	7DS03701	33.8	34.0	B-C	7.46	5.63	4.15	5.94	3.51	0.18	1.73	0.50	0.014
SCI-V-012	7DS03901	37.7	37.8	B-C	25.63	29.05	17.80	19.76	13.80	0.42	5.04	0.47	0.028
SCI-V-012	7DS08201	74.1	74.4	C-D	19.84	20.11	15.80	23.68	19.70	0.43	3.26	0.26	0.036
SCI-V-013	7DS04301	29.7	29.9	B-C	14.33	19.89	9.25	22.99	19.40	0.24	3.08	0.25	0.024
SCI-V-013	7DS04702	70.1	70.3	C-D	7.07	5.37	4.21	4.99	3.32	0.18	1.38	0.10	0.009
SCI-V-013	7DS04701	71.4	71.6	C-D	40.36	44.07	13.60	24.65	18.50	0.62	5.13	0.36	0.034
SCI-V-014	7DS08801	32.9	33.2	B-C	52.48	56.50	35.70	39.67	28.90	0.77	9.61	0.34	0.049
SCI-V-014	7DS08901	36.0	36.3	B-C	52.97	60.53	34.70	43.38	33.10	0.81	9.05	0.36	0.050
SCI-V-014	7DS09001	74.1	74.7	C-D	42.96	37.27	14.40	28.92	22.20	0.79	5.61	0.27	0.044
SCI-V-015	7DS08401	34.0	34.6	B-C	4.11	4.33	4.38	8.14	5.93	0.26	1.65	0.28	0.014
SCI-V-015	7DS08501	35.9	36.2	B-C	21.05	15.33	24.50	29.16	23.30	0.49	4.81	0.53	0.034
SCI-V-015	7DS08601	38.4	38.8	B-C	60.22	62.82	37.20	44.18	33.20	0.85	9.60	0.48	0.052
SCI-V-015	7DS08701	38.4	38.8	B-C	60.65	64.00	38.60	43.21	32.20	0.93	9.53	0.49	0.054
SCI-V-015	7DS08301	75.9	76.2	C-D	40.05	31.70	21.60	20.72	13.80	0.75	5.86	0.27	0.044
SCI-V-016	7DS09101	40.9	41.2	B-C	34.72	36.77	27.60	36.51	28.90	0.47	6.34	0.75	0.043
SCI-V-016	7DS09201	45.1	45.4	B-C	27.43	31.58	20.10	28.73	23.00	0.39	4.78	0.52	0.035
SCI-V-016	7DS09301	45.1	45.4	B-C	26.45	29.61	23.90	30.82	24.90	0.47	4.88	0.54	0.036
SCI-V-016	7DS09401	74.7	75.6	C-D	13.28	14.88	3.50	5.20	3.31	0.08	1.58	0.21	0.018
SCI-V-153	7DS00101	31.4	31.6	B-C	—	75.24	43.90	48.66	34.80	0.96	12.10	0.74	0.058
SCI-V-153	7DS00301	32.7	32.9	B-C	—	61.36	23.20	29.16	20.70	0.98	7.22	0.22	0.041
SCI-V-153	I1S- 109	33.2	33.4	B-C	—	26.32	25.50	53.46	46.10	0.96	5.81	0.55	0.051
SCI-V-154	7DS00701	31.4	31.6	B-C	—	19.29	14.80	12.88	9.58	0.32	2.75	0.20	0.024
SCI-V-154	I2S- 105	31.9	32.0	B-C	—	50.29	42.40	36.51	27.20	0.75	8.10	0.39	0.068
SCI-V-154	7DS00901	34.1	34.3	B-C	—	51.14	27.30	36.97	29.60	0.59	6.47	0.26	0.053
SCI-V-157	I3D- 229	69.9	70.0	C-D	—	24.75	15.80	47.83	42.50	0.77	4.11	0.41	0.048

Table 2. (continued).

Well ID	Sample ID	Interval Top (m bls)	Interval Bottom (m bls)	Interbed	Surface Area INEEL (m^2/g)	Surface Area SWRI (m^2/g)	CEC (meq/100g)	Calc CEC (meq/100g)	Exch Ca (meq/100g)	Exch K (meq/100g)	Exch Mg (meq/100g)	Exch Na (meq/100g)	Exch Sr (meq/100g)
SCI-V-157	7DS01701	70.4	70.6	C-D	—	36.58	23.20	27.75	21.10	0.63	5.70	0.28	0.043
SCI-V-159	I4D-224	68.4	68.5	C-D	—	32.76	17.60	46.45	39.90	0.93	5.08	0.49	0.057
SCI-V-159	7DS02301	70.1	70.3	C-D	—	34.02	22.50	23.80	16.70	0.68	6.11	0.27	0.040
SCI-V-159	I4D- 231	70.3	71.2	C-D	—	31.81	20.60	40.25	33.60	1.07	5.01	0.53	0.043
SCI-V-159	I4D- 234	71.2	71.3	C-D	—	17.16	13.80	19.21	14.70	0.71	3.44	0.34	0.025
SCI-V-160	I1D--234	71.3	71.5	C-D	—	50.53	29.50	25.41	18.40	1.38	5.23	0.35	0.048
SCI-V-160	7DS00501	72.6	72.7	C-D	—	46.39	19.40	31.29	24.70	1.49	4.78	0.28	0.043

Table 3. Material property results, extractable oxides, and partition coefficients for uranium and neptunium.

Well ID	Sample ID	Interval Top (m bls)	Interval Bottom (m bls)	Interbed	Ext SiO_2 (mg/g sed)	Ext Al_2O_3 (mg/g sed)	Ext Fe_2O_3 (mg/g sed)	Ext MnO_2 (mg/g sed)	Np Kd (mL/g)	U Kd (mL/g)
MON-A-009	7DS09501	41.5	41.9	B-C	0.88	0.35	6.66	0.56	6	18
MON-A-009	7DS09601	44.1	44.4	B-C	1.25	0.58	7.86	0.17	41	15
MON-A-009	7DS09701	69.8	70.1	C-D	3.29	1.48	15.00	0.13	22	12
SCI-V-011	7DS03101	31.7	31.9	B-C	2.62	0.88	15.40	0.41	17	17
SCI-V-011	7DS03301	33.5	33.8	B-C	1.56	0.77	8.96	0.26	32	15
SCI-V-011	7DS03501	71.6	71.8	C-D	2.57	1.08	15.80	0.39	28	34
SCI-V-012	7DS03701	33.8	34.0	B-C	0.61	0.28	5.45	0.16	4	3
SCI-V-012	7DS03901	37.7	37.8	B-C	1.38	0.69	8.45	0.43	8	18
SCI-V-012	7DS08201	74.1	74.4	C-D	1.39	0.43	8.80	0.15	17	16
SCI-V-013	7DS04301	29.7	29.9	B-C	1.01	0.45	5.55	0.14	140	11
SCI-V-013	7DS04702	70.1	70.3	C-D	0.29	0.25	5.68	0.15	0.3	8
SCI-V-013	7DS04701	71.4	71.6	C-D	1.89	0.69	5.58	0.23	18	11
SCI-V-014	7DS08801	32.9	33.2	B-C	2.12	1.10	13.00	0.63	29	27
SCI-V-014	7DS08901	36.0	36.3	B-C	2.58	1.07	8.96	0.64	47	30
SCI-V-014	7DS09001	74.1	74.7	C-D	1.99	0.84	8.70	0.29	39	17
SCI-V-015	7DS08401	34.0	34.6	B-C	0.71	0.31	4.96	0.17	0.02	1
SCI-V-015	7DS08501	35.9	36.2	B-C	1.37	0.59	6.47	0.36	45	13
SCI-V-015	7DS08601	38.4	38.8	B-C	2.44	1.07	10.40	0.92	29	32
SCI-V-015	7DS08701	38.4	38.8	B-C	2.29	1.05	10.10	0.84	25	33
SCI-V-015	7DS08301	75.9	76.2	C-D	1.55	0.70	7.13	0.24	11	48
SCI-V-016	7DS09101	40.9	41.2	B-C	1.27	0.70	7.39	0.58	74	27
SCI-V-016	7DS09201	45.1	45.4	B-C	1.96	0.91	11.40	0.50	40	27
SCI-V-016	7DS09301	45.1	45.4	B-C	1.83	0.90	11.50	0.52	37	26
SCI-V-016	7DS09401	74.7	75.6	C-D	2.96	1.29	12.80	0.14	0.4	5
SCI-V-153	7DS00101	31.4	31.6	B-C	2.84	0.93	16.60	0.66	85	19
SCI-V-153	7DS00301	32.7	32.9	B-C	2.17	1.06	10.20	0.57	38	30
SCI-V-153	I1S-109	33.2	33.4	B-C	3.76	1.56	10.30	0.36	233	19
SCI-V-154	7DS00701	31.4	31.6	B-C	1.19	0.49	5.90	0.14	8	17
SCI-V-154	I2S -105	31.9	32.0	B-C	3.55	1.34	10.10	0.29	23	25
SCI-V-154	7DS00901	34.1	34.3	B-C	1.72	0.82	8.46	0.41	50	26

Table 3. (continued).

Well ID	Sample ID	Interval Top (m bls)	Interval Bottom (m bls)	Interbed	Ext SiO2 (mg/g sed)	Ext Al2O3 (mg/g sed)	Ext Fe2O3 (mg/g sed)	Ext MnO2 (mg/g sed)	Np Kd (mL/g)	U Kd (mL/g)
SCI-V-157	I3D -229	69.9	70.0	C-D	5.21	1.84	12.40	0.21	251	15
SCI-V-157	7DS01701	70.4	70.6	C-D	1.93	0.73	14.50	0.26	77	24
SCI-V-159	I4D-224	68.4	68.5	C-D	4.53	2.26	18.30	0.31	100	19
SCI-V-159	7DS02301	70.1	70.3	C-D	2.62	0.83	12.90	0.27	52	23
SCI-V-159	I4D -231	70.3	71.2	C-D	6.24	2.00	14.10	0.26	59	16
SCI-V-159	I4D -234	71.2	71.3	C-D	3.97	1.41	10.40	0.26	27	11
SCI-V-160	I1D -234	71.3	71.5	C-D	4.22	2.20	12.40	0.65	40	29
SCI-V-160	7DS00501	72.6	72.7	C-D	1.52	0.92	5.56	0.35	80	21

Table 4. Composition of simulated groundwater used in experiments to measure uranium adsorption.

Component	Concentration (mmol/L)	Concentration (mg/L)
Ca^{+2}	1.27	51
Mg^{+2}	0.74	18
Na^{+}	7.87	181
K^{+}	0.10	3.9
HCO_3^{-}	3.61	220
SO_4^{-2}	0.43	41
Cl^{-}	7.60	270
F^{-}	0.03	0.6
pH	8.0 ± 0.2	

Table 5. Initial isotope tracer concentrations in test solutions for uranium and neptunium.

	Uranium-233		Neptunium-237	
	Bq/mL	µmol/L	Bq/mL	µmol/L
1	8.8	0.105	4.9	0.79
2	21.9	0.264	12.3	1.99
3	37.8	0.454	24.5	3.96
4	75.6	0.908	48.5	7.84
5	175.6	2.11	95.1	15.4

After equilibration, the test solutions were centrifuged at 1,000 g for 5 minutes and an aliquot collected for counting of the isotope tracer remaining in solution. The partition coefficient was calculated using:

$$K_d = \frac{(C_i - C_e)}{C_e}\frac{v}{m} \tag{2}$$

where

C_i = initial solution concentration of isotope (Bq/mL)

C_e = equilibrium solution concentration of isotope (Bq/mL)

v = volume of test solution (mL)

m = mass of suspended solids (g).

Sorption was measured at five concentrations of tracer and was nonlinear with a decrease in the sorption efficiency as the solution concentration increased. This decrease in sorption efficiency was well

described by a Freundlich isotherm (Ayaz et al. 2003; Hull et al. 2003). For performance assessment and risk assessment modeling at the SDA, the simpler linear sorption isotherm (K_d) is used. To make this assessment of K_d representative of expected sorption conditions at the SDA, natural uranium concentration in the SDA pore water must be included in calculated partitioning in addition to uranium from contamination. Sorption decreases with increasing uranium concentration; therefore, the background concentration will affect the partitioning of uranium. Natural uranium concentrations in the pore water in the vadose zone at the SDA were measured using thermal ionization mass spectrometry (Roback et al. 2000). Natural uranium concentrations range from 0.01 to 0.6 μmol/L. Comparing these values to the experimental concentrations listed in Table 5 indicates that the three lowest concentrations used in the isotherm experiments are the most representative of subsurface conditions at the SDA for uranium. Rather than select the K_d value measured at the lowest solution concentration, the three lowest measured points of the sorption data were fit using a linear isotherm with a zero intercept to determine a single K_d value for each sample (see Table 3). Fitting the sorption at the three lowest uranium concentrations provides a smaller value of K_d than using the K_d measured at the lowest concentration only and is more representative of conditions at the SDA. Even though there are no natural background concentrations of neptunium, linear fitting of the three lowest concentrations was also used to determine neptunium K_d values for comparability. The K_d values calculated from the linear fits were corrected to the total sample weight by adjusting for the gravel fraction removed by sieving out material greater than 2 mm.

Two of the cores were selected to evaluate the reproducibility of the isotherm measurements. Each of the two core intervals was homogenized, split, and submitted to the laboratory as two separate samples for measurement of sorption isotherms. The core intervals were from well SCI-V-015 at a depth of 38.4 m and from well SCI-V-016 from a depth of 45.1 m (see Table 3). The agreement between the K_d values from the measured adsorption isotherms is very good. Relative percent difference for neptunium K_d values was 4% and 2%, and for uranium K_d values was –1% and 1%. Laboratory methods provide very good reproducibility of K_d values.

2.3 Statistical Analysis Methods

The distributions of the K_d values for neptunium and uranium were tested for normality using the Shapiro-Wilk test (Shapiro and Wilk 1965). If the data were significantly non-normal, then the log-transformed data were also tested for a lognormal distribution using the Shaprio-Wilk test. The coefficient of variance (CV) was calculated to help ascertain distribution. Koch and Link (1980) suggest that data with a CV less than 1.2 do not require log transformation.

The K_d values and other measured covariates were compared between the interbeds and also investigated for a relationship with depth. The data were initially compared using a nested analysis of variance (ANOVA). The nested ANOVA was used because the relative difference between interbeds at each site was of interest, not necessarily the absolute difference in measurements from the interbeds. The sources of variance for the ANOVA were the wells and the interbeds nested within the wells. The data were also compared in a non-nested approach by simply comparing the data from interbeds using either a t-test (Snedecor and Cochran 1980) or Wilcoxon rank sum test (Conover 1980) for independent samples and their paired analogs (i.e., paired t-test and Wilcoxon signed-rank test) for wells that had samples from both interbeds. The t-tests were used for normally distributed data and the Wilcoxon tests for data that were not normal or lognormal. The paired tests were based on the mean value from each interbed if more than one sample was collected and analyzed at a surface location within an interbed. The K_d values were also investigated for correlation between the interbeds. If low K_d values in the B-C interbed were related to low values in the C-D interbed, this might support the hypothesis of fast-flow zones existing through the vadose zone interbed layers. This correlation analysis was only possible for wells with samples from both interbeds.

All sediment characteristics were investigated using Spearman's correlation coefficient (Snedecor and Cochran 1980) and polynomial regression using the best predictor and regression trees (Breiman et al. 1984) to determine predictive equations. The best predictor was selected as the variable with the largest correlation. A stepwise polynomial regression was run to determine the optimal regression equation using only one predictor. Regression trees are a nonparametric approach to prediction. Regression tree models are fit by successively splitting the data to form homogeneous subsets. The result is a hierarchical tree of decision rules useful for prediction. The regression tree approach was selected to investigate prediction of K_d values from sediment characteristics because it can easily handle a large number of predictors, it is robust to correlations among predictors, it can incorporate categorical (e.g., interbed) and continuous data, and it makes no distributional assumptions. The tree model predictions are based on the series of splits. The resulting prediction is the mean of the responses for observations in that final branch or node. The predictions from the polynomial regression and regression tree model were summarized and compared by the standard deviation of the predictions compared to the measured data, the standard deviation of the residuals, the minimum and maximum of the residuals, the number of positive and negative residuals, the mean square error (MSE), MSE as percent of the measured K_d, the mean absolute value of the residuals, correlation between prediction and measured K_d, and the Shapiro-Wilk test for normality p-value.

Kriging (Ripley 1981; Cressie 1993) was used to predict K_d values for each interbed. Kriging makes predictions based upon a weighted mean of all sample values. Kriging predictions minimize the error variance by weighting observations based on the variogram model parameters. The variogram is the matched values of distance and pairwise semi-variance at that distance. The empirical variogram, which averages within a distance tolerance, is fit with a model whose parameters are used in the kriging equations. Based on the variogram parameters, those values closer to the prediction locations receive larger weight. These values are more highly correlated with the predictions site, resulting in smaller prediction variance.

Kriging makes two assumptions: (1) there is a locally common expected value (stationarity), and (2) spatial correlation is independent of direction (isotropy). Stationarity is assumed for simple kriging, local stationarity is assumed for ordinary kriging, and stationarity after large-scale trend removal is assumed for universal kriging. Large-scale trend of the K_d values was investigated through polynomial regression on easting and northing. If no large-scale trend exists, then local ordinary kriging was performed. Isotropy is generally investigated through the directional variograms. Directional variograms limit the pairs to be within a tolerance of a specified angle of each other. With only nine or ten sample locations in each interbed, the sample data were insufficient to calculate directional variograms by interbed; therefore, isotropy was assumed without confirmation.

Two forms of the variogram are investigated to develop a model: (1) classical empirical variograms, and (2) variogram clouds. The empirical variogram is the mean semi-variance for pairs of locations within some tolerance of a given lag distance. The variogram cloud is a scatter plot of all possible pairwise variances. For n=10 there are 45 pairwise semi-variances. The variogram cloud is useful in determining the range, especially when sample size is small, but the number of pairwise semi-variances quickly becomes overwhelming with a large sample size. The classical empirical variogram provides a summary of the pairwise semi-variances and is used to model the average spatial correlation behavior.

The empirical variograms and variogram clouds were calculated for the data separately by interbed. If there was more than one result per interbed, the mean of the results was used for variogram calculation. The variograms were modeled by specifying a model that describes the shape (e.g., spherical or exponential), nugget (i.e., small-scale variation), sill (i.e., asymptotic variance between pairs of independent sites), and range (i.e., distance at which the sill is attained).

Ideally, 3-D spatial models would be applied to the K_d sample values. There are limited samples at depth; therefore, 2-D kriging was applied for each interbed. Kriging requires one value per horizontal location, so the mean result was used for multiple interbed results. The predictions are made for a base grid and one grid refinement for the B-C interbed, and only the base grid for the C-D interbed. The grid refinement is rectangular and of smaller domain size and greater descritization intensity than the base grid (see Figure 2). This follows the pattern of data needs for hydrologic modeling as discussed above. For input to the computer simulation model of the vadose zone, the predictions on Grid 1 (i.e., the refinement grid used for the B-C interbed) override the predictions made on the base grid. Variogram calculation and modeling and kriging were implemented using the S+SpatialStats module in S-Plus (Release 2, Insightful Inc., Seattle, WA).

3. RESULTS

The results are presented for neptunium and uranium K_d values for each type of statistical analysis: distribution of values, differences between interbeds, correlation and regression among variables, and spatial modeling.

3.1 Sorption Coefficients

The distribution of neptunium K_d was highly skewed (see Figure 5) and the distribution of uranium K_d was slightly skewed (see Figure 6). The distribution of neptunium K_d was significantly non-normal (Shaprio-Wilk p-value < 0.0001), and non-lognormal (Shapiro-Wilk p-value < 0.0001) (see Figure 7). The log transformation resulted in a few very small values that skewed the distribution left (see Figure 7). The CV for neptunium K_d was 1.0, indicating a log transformation may not be necessary. Because the distribution of neptunium K_d was indeterminate, raw data and log-transformed values were used for spatial modeling. The distribution of uranium K_d did not significantly differ from normality (Shaprio-Wilk p-value = 0.46). The CV for uranium K_d was 0.5, far below the recommended guideline of 1.2. Uranium and neptunium K_d values were not correlated with each other (r = 0.3) at the 5% significance level suggesting that sorption of these two elements is related to different material properties of the sediments.

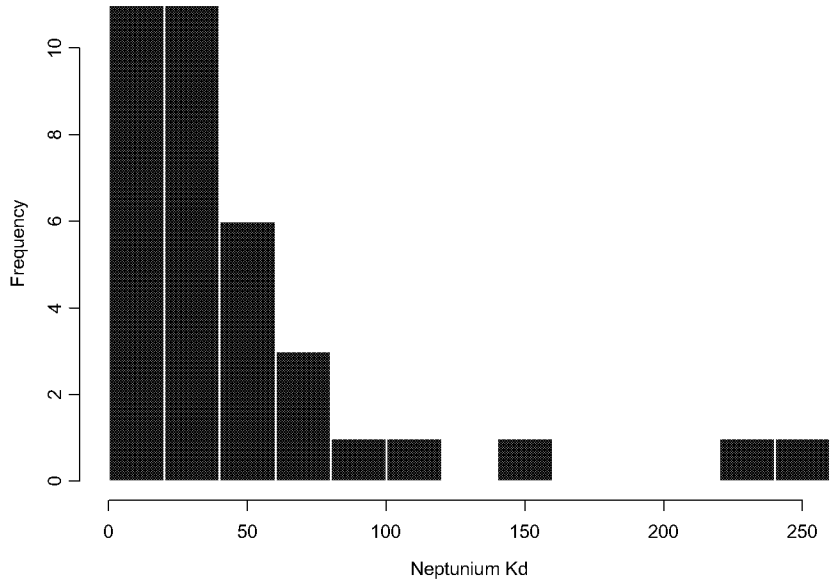

Figure 5. Histogram of neptunium K_d (mL/g) values.

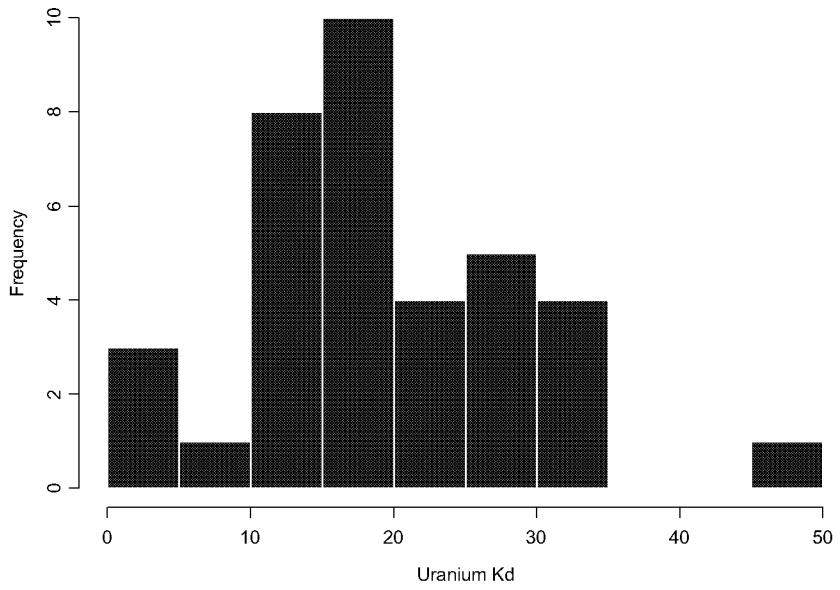

Figure 6. Histogram of uranium K_d (mL/g) values.

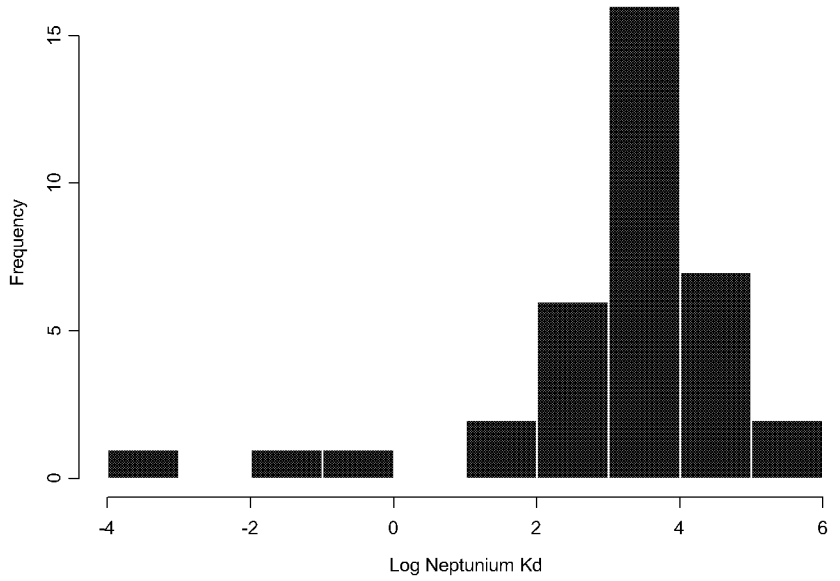

Figure 7. Histogram of log-transformed neptunium K_d (mL/g) values.

3.2 Variation Between Interbeds

There is no evidence that neptunium K_d (see Figure 8) differs between interbeds, but there is some evidence that uranium K_d (see Figure 9) does differ between interbeds. For neptunium, where samples were collected from both the B-C and C-D interbeds from the same well (O-1, O-2, O-5, O-6, and M15S), the K_d values from the wells plot together. There are some notable exceptions such as for wells O-3 and O-7. For uranium, the K_d values are more separated between interbeds in wells O-1, O-5, O-6, O-7, and O-8. The uranium K_d values are similar between interbeds only in wells O-2 and O-3. The ANOVA test was not significant for interbed nested within well for neptunium K_d (see Table 6), but was significant for uranium K_d (see Table 7). Thus, the uranium K_d values for any particular well were generally lower for

the C-D interbed than they were for the B-C interbed. For neptunium K_d, the Wilcoxon rank sum test for differences between interbeds was not significant (p-value > 0.8), and the paired Wilcoxon signed-rank test was also not significant (p-value = 0.4) based on 7 wells with paired results. For uranium K_d, the t-test for differences between interbeds was not significant (p-value = 0.9), and the paired t-test was also not significant (p-value = 0.7) based on 7 wells with paired results. Thus, the overall sorption did not differ by interbed, but, as shown by the nested ANOVA results, interbed differences for uranium K_d may be significant on a well-specific basis (see Table 8). Depth was not correlated to either the neptunium or uranium K_d (see Table 9).

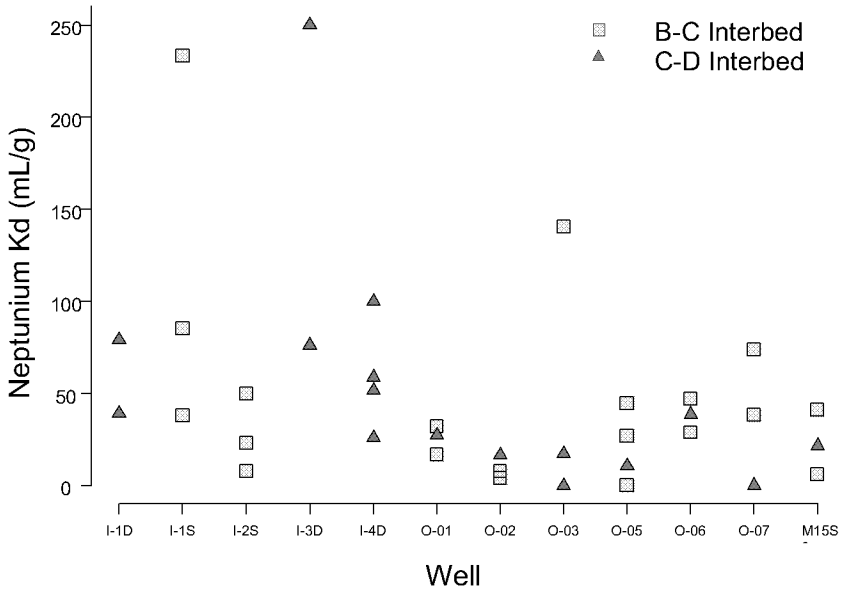

Figure 8. Neptunium K_d (mL/g) for wells by interbed.

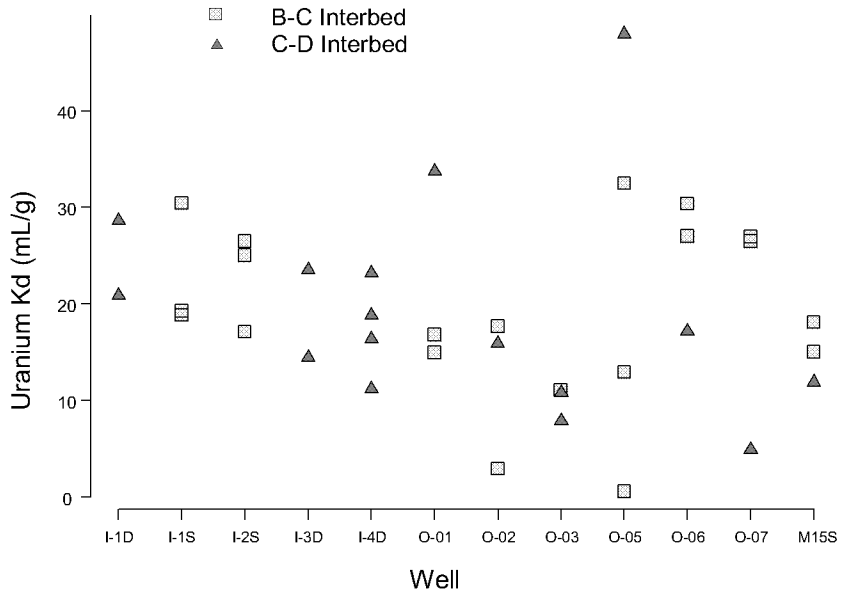

Figure 9. Uranium K_d (mL/g) for wells by interbed.

Table 6. Analysis of variance table for neptunium K_d (mL/g).

Source	Degrees of Freedom	Sums of Squares	Mean Square	F = MSsource/MSE	P-value
Wells		55,444	5040	1.99	0.10
Interbed (Well)		13,803	1972	0.78	0.61
Unexplained/Residual		43,123	2537 = MSE		
Total		112,370			

Table 7. Analysis of variance table for uranium K_d (mL/g).

Source	Degrees of Freedom	Sums of Squares	Mean Square	F = MSsource/MSE	P-value
Wells	11	801	73	1.33	0.29
Interbed (well)	7	1453	208	3.78	0.01
Unexplained/residual	17	927	55 = MSE		
Total	35	3,181			

Table 8. Summary statistics for K_d values.

	Neptunium K_d		Uranium K_d	
Statistic	B-C Interbed	C-D Interbed	B-C Interbed	C-D Interbed
Minimum	5.8	0.4	10.3	5.0
Median	26.9	24.9	16.6	17.4
Maximum	140.4	163.6	28.7	48.0
Lower confidence limit	14.8	6.8	13.8	11.3
Mean	50.9	40.9	18.9	20.3
Upper confidence limit	87.0	75.0	24.0	29.3
Sample size	9	10	9	10
Value used in Holdren et al. (2002)	8	8	6	6

Table 9. Spearman correlation coefficients among measured covariates. Bold values are significant at the 0.05 level of significance.

	Depth	Np K_d	U K_d	Clay	Silt	Sand	Gravel
Neptunium K_d	-0.1	—	—	—	—	—	—
Uranium K_d	0.0	0.3	—	—	—	—	—
Clay	-0.1	0.0	**0.4**	—	—	—	—

Table 9. (continued).

	Depth	Np K_d	U K_d	Clay	Silt	Sand	Gravel
Silt	**0.5**	0.2	0.2	0.3	—	—	—
Sand	-0.1	-0.1	**-0.4**	**-0.8**	**-0.5**	—	—
Gravel	**-0.5**	-0.1	-0.2	-0.1	**-0.5**	0.2	—
Smectite clay	**-0.7**	-0.1	0.0	0.3	-0.3	-0.1	0.3
Illite clay	**0.8**	-0.1	-0.1	**-0.4**	0.3	0.2	**-0.4**
Kaolinite clay	-0.1	0.1	0.3	**0.5**	-0.1	**-0.5**	0.1
Smectite sed.	-0.2	0.0	**0.4**	**0.9**	0.3	**-0.8**	-0.1
Illite sed.	0.1	0.0	**0.4**	**0.9**	**0.4**	**-0.7**	-0.2
Kaolinite sed.	-0.2	0.0	**0.4**	**0.9**	0.2	**-0.7**	-0.1
Surface area	-0.1	**0.4**	**0.7**	0.3	0.1	**-0.4**	-0.1
CEC	**-0.3**	**0.4**	**0.8**	0.3	0.0	**-0.4**	-0.1
Exch. Ca	-0.3	**0.8**	**0.4**	0.1	0.2	-0.3	-0.2
Exch. K	0.1	**0.6**	**0.6**	-0.1	0.1	-0.1	-0.1
Exch. Mg	-0.3	**0.4**	**0.7**	**0.4**	0.1	**-0.5**	-0.1
Exch. Na	-0.2	0.3	0.1	0.0	0.1	-0.1	0.0
Exch. Sr	-0.1	**0.6**	**0.7**	0.1	0.1	-0.2	-0.2
Ext. SiO_2	0.2	**0.4**	0.3	**-0.4**	0.0	0.2	**-0.4**
Ext. Al_2O_3	0.1	**0.4**	**0.3**	**-0.4**	0.0	0.2	**-0.4**
Ext. Fe_2O_3	0.1	0.3	**0.3**	-0.3	0.0	-0.0	**-0.4**
Ext. MnO_2	-0.2	0.4	**0.7**	0.3	0.1	**-0.5**	0.0

	Sm. Clay	Illite Clay	Kao. Clay	Sm. Sed.	Illite Sed.	Kao. Sed.	Surf. Area	CEC
Neptunium K_d	—	—	—	—	—	—	—	—
Uranium K_d	—	—	—	—	—	—	—	—
Clay	—	—	—	—	—	—	—	—
Silt	—	—	—	—	—	—	—	—
Sand	—	—	—	—	—	—	—	—
Gravel	—	—	—	—	—	—	—	—
Smectite clay	—	—	—	—	—	—	—	—
Illite clay	**-0.9**	—	—	—	—	—	—	—
Kaolinite clay	-0.0	-0.3	—	—	—	—	—	—
Smectite sed.	**0.4**	**-0.4**	**0.5**	—	—	—	—	—

Table 9. (continued).

	Sm. Clay	Illite Clay	Kao. Clay	Sm. Sed.	Illite Sed.	Kao. Sed.	Surf. Area	CEC
Illite sed.	0.0	-0.1	**0.4**	**0.9**	—	—	—	—
Kaolinite sed.	0.3	**-0.5**	**0.7**	**0.9**	**0.9**	—	—	—
Surface area	0.1	-0.2	0.0	0.3	0.3	0.2	—	—
CEC	**0.4**	**-0.5**	0.2	0.3	0.2	**0.4**	**0.8**	—
Exch. Ca	0.2	-0.3	0.0	0.1	0.0	0.1	**0.6**	**0.7**
Exch. K	-0.2	0.1	-0.1	-0.1	-0.0	-0.1	0.7	0.6
Exch. Mg	**0.4**	**-0.4**	0.2	**0.4**	0.3	**0.4**	**0.8**	**0.9**
Exch. Na	0.1	-0.2	0.1	0.0	-0.1	0.0	0.1	0.3
Exch. Sr	0.2	-0.2	-0.1	0.1	0.1	0.1	0.8	0.8
Ext. SiO_2	-0.2	0.2	-0.2	**-0.4**	-0.3	**-0.4**	**0.4**	**0.4**
Ext. Al_2O_3	-0.3	0.2	-0.2	**-0.4**	-0.3	-0.3	**0.5**	**0.4**
Ext. Fe_2O_3	-0.2	0.1	0.0	-0.3	-0.3	-0.2	**0.4**	**0.4**
Ext. MnO_2	0.2	-0.3	0.1	0.3	0.3	0.3	**0.8**	**0.8**

	Exch. Ca	Exch. K	Exch. Mg	Exch. Na	Exch. Sr	Ext. SiO_2	Ext. Al_2O_3	Ext. Fe_2O_3
Neptunium K_d	—	—	—	—	—	—	—	—
Uranium K_d	—	—	—	—	—	—	—	—
Clay	—	—	—	—	—	—	—	—
Silt	—	—	—	—	—	—	—	—
Sand	—	—	—	—	—	—	—	—
Gravel	—	—	—	—	—	—	—	—
Smectite clay	—	—	—	—	—	—	—	—
Illite clay	—	—	—	—	—	—	—	—
Kaolinite clay	—	—	—	—	—	—	—	—
Smectite sed.	—	—	—	—	—	—	—	—
Illite sed.	—	—	—	—	—	—	—	—
Kaolinite sed.	—	—	—	—	—	—	—	—
Surface area	—	—	—	—	—	—	—	—
CEC	—	—	—	—	—	—	—	—
Exch. Ca	—	—	—	—	—	—	—	—
Exch. K	**0.7**	—	—	—	—	—	—	—
Exch. Mg	**0.6**	**0.6**	—	—	—	—	—	—

Table 9. (continued).

	Exch. Ca	Exch. K	Exch. Mg	Exch. Na	Exch. Sr	Ext. SiO_2	Ext. Al_2O_3	Ext. Fe_2O_3
Exch. Na	**0.5**	0.2	0.2	—	—	—	—	—
Exch. Sr	**0.8**	**0.8**	**0.8**	0.3	—	—	—	—
Ext. SiO_2	**0.5**	**0.6**	**0.3**	0.1	**0.6**	—	—	—
Ext. Al_2O_3	**0.5**	**0.7**	0.3	0.1	**0.6**	**0.9**	—	—
Ext. Fe_2O_3	**0.4**	**0.5**	**0.4**	0.0	**0.5**	**0.8**	**0.8**	—
Ext. MnO_2	**0.6**	**0.7**	**0.8**	**0.4**	**0.7**	**0.3**	**0.4**	**0.4**

There are only two measured covariates that significantly differ between the interbeds: smectite fraction (g/g of clay) (Wilcoxon test p-value < 0.0001) and illite fraction (g/g of clay) (Wilcoxon test p-value < 0.0001). Samples collected from the shallower interbed, the B-C interbed, have a broad range of textural characteristics ranging from sand to clay (see Figure 10). Samples collected from the C-D interbed primarily consist of silt and sand and do not contain as much clay-sized material as found in the B-C interbed samples. The suite of clay minerals identified in the samples, illite, smectite, and kaolinite, are consistent with results of previous mineralogic investigations (Rightmire and Lewis 1987; Bartholomay et al. 1989; Bartholomay 1990) and are similar for both interbeds. However, the relative quantities of the clays are very different. Samples from the B-C interbed have about five times as much smectite as illite, while samples from the C-D interbed have about equal amounts of smectite and illite (see Figure 11). These differences are based on the samples that were recovered and analyzed, but the results may have bias because of the sample recovery issues and subsectioning methods described above.

There was no significant correlation between the K_d values from the B-C and C-D interbeds. The small negative correlations (i.e., -0.37 for neptunium and –0.22 for uranium) were due to a couple of large results. Without these large results, there was a positive correlation for neptunium K_d ($r = 0.7$ for $n = 5$) that was not significantly different from zero (p-value >0.1) given the small sample size. The correlation for uranium K_d (-0.17, $n = 5$) was closer to 0 without the large results.

3.3 Correlations Among Material Properties

The correlations among the covariates are shown in Table 9. Neptunium K_d was positively correlated with surface area, sum of exchangeable cations (CEC in meq/100g), exchangeable Ca, K, Mg, and Sr (meq/100g), and extractable SiO_2, Al_2O_3, and MnO_2 (mg/g of sediment). Uranium K_d was positively correlated with clay, smectite, illite, and kaolinite fractions (g/g of sediment), surface area (m^2/g), sum of exchangeable cations (CEC in meq/100g), exchangeable Ca, K, Mg, and Sr (meq/100g), and extractable Al_2O_3, Fe_2O_3, and MnO_2 (mg/g of sediment). Uranium K_d was negatively correlated with sand fraction (g/g of sediment). Depth was significantly positively correlated to silt fraction (g/g of sediment) and illite fraction (g/g of clay) and significantly negatively correlated with gravel fraction (g/g of sediment), smectite fraction (g/g of clay), and sum of exchangeable cations (CEC in meq/100g). There were other groups of correlations as well. Surface area (m^2/g) and sum of exchangeable cations (CEC in meq/100g) were positively correlated with the exchangeable cations and extractable compounds, which were generally significantly positively correlated among themselves as well.

To determine if measurement of geochemical material properties could be used to predict uranium and neptunium sorption using lower cost and more readily measured parameters, regression analysis was used to evaluate the prediction of K_d values from material properties. Uranium K_d was

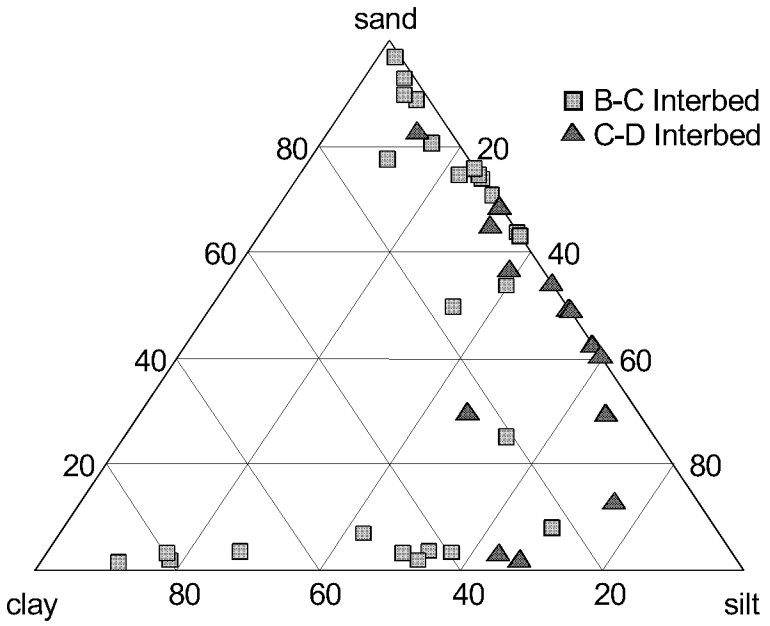

Figure 10. Grain size distribution for all samples collected from the sedimentary interbeds. The B-C interbed is more evenly distributed between sand, silt, and clay, while the C-D interbed is much lower in clay content.

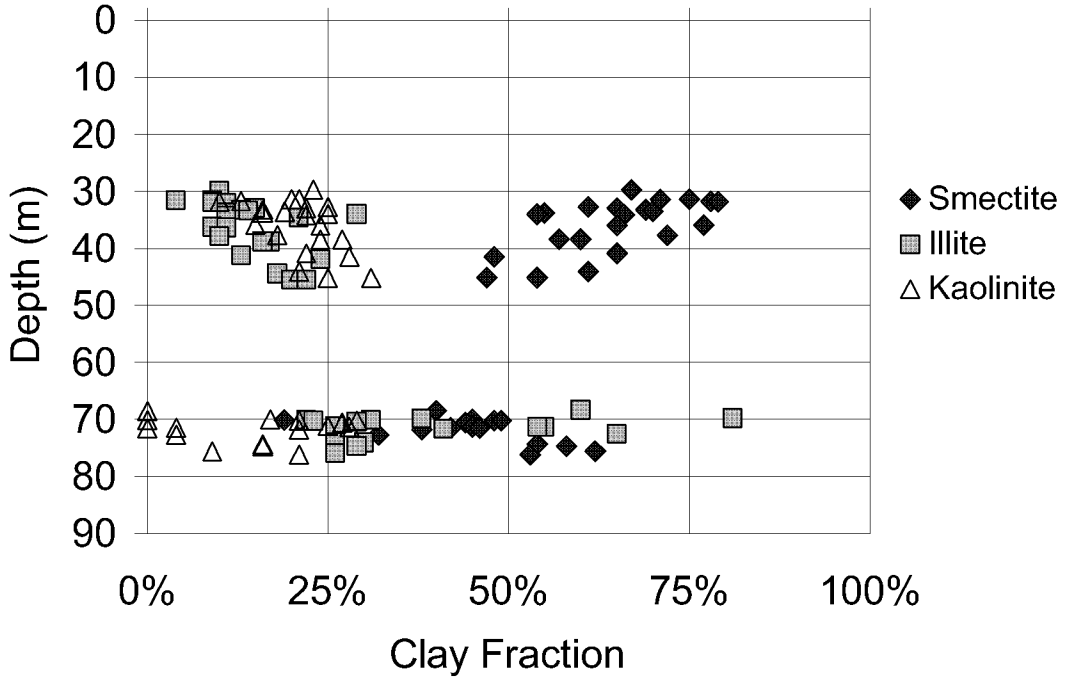

Figure 11. Clay mineral composition of the B-C and C-D interbeds.

most highly correlated with the sum of exchangeable cations (CEC in meq/100g), so that was chosen as the most likely material property to predict the uranium K_d. The polynomial regression resulted in significant (t-test p-value < 0.05) coefficients for CEC and CEC^2, but not CEC^3 (t-test p-value > 0.05). The quadratic regression equation for uranium was:

$$K_d = -1.4 + 1.7CEC - 0.03CEC^2. \quad (3)$$

The R^2 was 54%, indicating that the regression explained about half of the variability in the uranium K_d. The residual plots, not shown, support the assumptions of independence and homoscedasticity. The Shaprio-Wilk test does not support the assumption of normally distributed residuals (see Table 10).

Table 10. Polynomial regression and regression tree model fit measures.

	Polynomial Regression		Regression Tree	
Measure	Neptunium K_d	Uranium K_d	Neptunium K_d	Uranium K_d
Standard deviation of data	56.7	9.5	56.7	9.5
Standard deviation of predictions	56.1	7.0	55.3	9.4
Standard deviation of residuals	34.0	6.5	12.2	2.3
Minimum residual	-96.3	-11.5	-30.4	-7.1
Maximum residual	108.9	25.1	30.4	7.1
Number of positive residuals	21	15	20	17
Number of negative residuals	15	21	16	16
Median squared error	1151.9	7.7	75.5	1.6
Median squared error as % of truth	1732%	47%	269%	8%
Mean absolute residual	19.7	4.3	9.6	1.5
Correlation between truth and prediction	0.82	0.73	0.98	0.96
Shaprio-Wilk p-value for residuals	0.00002	0.001	0.11	0.02

Neptunium K_d was most highly correlated with exchangeable Ca (ExCa in meq/100g; therefore, it was selected as the most likely material property to predict the neptunium K_d. The neptunium K_d values were log-transformed to attain symmetry, but not normality, as discussed above. The cubic regression, with all significant terms (t-test p-values < 0.05), was:

$$\log(K_d) = -2.2 + 0.6\ ExCa - 0.02ExCa^2 + 0.0003ExCa^3. \quad (4)$$

The R^2 was 65%, indicating that the regression explained more than half of the variation in log (neptunium K_d). The residual plots, not shown, support the assumptions of independence and homoscedasticity. The Shapiro-Wilk test does not support the assumption of normally distributed residuals (see Table 10). The predictions were simply exponential back-transformed to calculate comparison measures, without adjusting for bias by adding a fraction of the variance, which follows the recommended approach used for kriging, described below.

A second approach to predicting K_d values was the use of regression trees. Based on the regression tree, the important variables for predicting neptunium K_d were the exchangeable calcium (ExCa in meq/100g), extractable iron (mg Fe_2O_3/g sediment), kaolinite fraction (g/g of sediment), and sum of exchangeable cations (CEC meq/100 g). Note that the length of the vertical branches below the

split represents the predictive potential of that variable so that exchangeable calcium was the only major contributor (see Figure 12). The standard deviation of the data is approximately equal to the standard deviation of the predicted values, the predicted values are highly correlated with the measured values, and there are no large outliers (see Table 10).

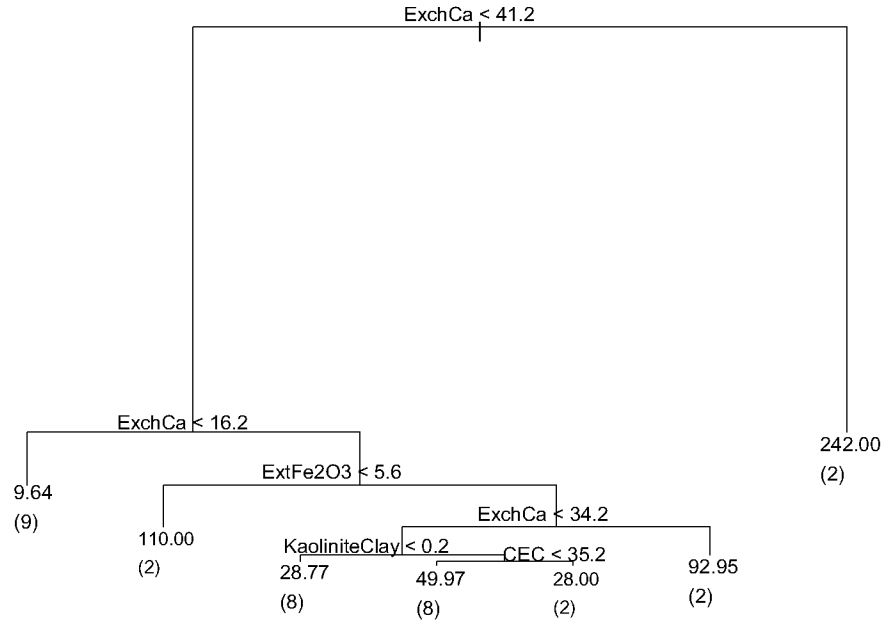

Figure 12. Regression tree for neptunium K_d. Significant predictors are exchangeable Ca (ExchCa), extractable Fe_2O_3 (ExtFe2O3), kaolinite fraction of clay (KaoliniteClay), and sum of exchangeable cations (CEC). Predicted neptunium K_d is given at nodes with number of observations per category in parentheses. Length of vertical line below node represents importance of that predictor.

Based on the regression tree, the important variables for predicting uranium K_d were the calculated sum of exchangeable cations (CEC in meq/100g), exchangeable calcium and magnesium ions (meq/100 g), extractable oxides of iron and manganese (mg/g sediment), silt fraction (g/g sediment), and clay mineralogy. Again, the length of the vertical branches below the split represents the predictive potential of that variable, so the major contributors were the calculated sum of exchangeable cations, exchangeable calcium and magnesium ions, and extractable oxides of manganese (see Figure 13). The standard deviation of the data is approximately equal to the standard deviation of the predicted values, indicating that the natural variability is preserved (see Table 10). Also, the predicted values are highly correlated with the measured values and there are no large outliers (see Table 10).

Both uranium and neptunium sorption are correlated to ion exchange characteristics of the sediments. Studies of uranium sorption to clays show that uranium is bound both by ion exchange to fixed charge sites, and by formation of surface complexes at the edges of clay mineral sheets (McKinley et al. 1995; Sylwester et al. 2000; Chisholm-Brause et al. 2001). Neptunium is also sorbed to clays (Bertetti et al. 1998). Neptunium and uranium are also known to sorb strongly to iron and manganese oxides (Waite et al. 1994; Davis et al. 1998; Bargar et al. 1999; Kohler et al. 1999; Barnett et al. 2002), and the correlation of the K_d values to extractable iron suggests that iron minerals contribute sorption in INEEL sediments.

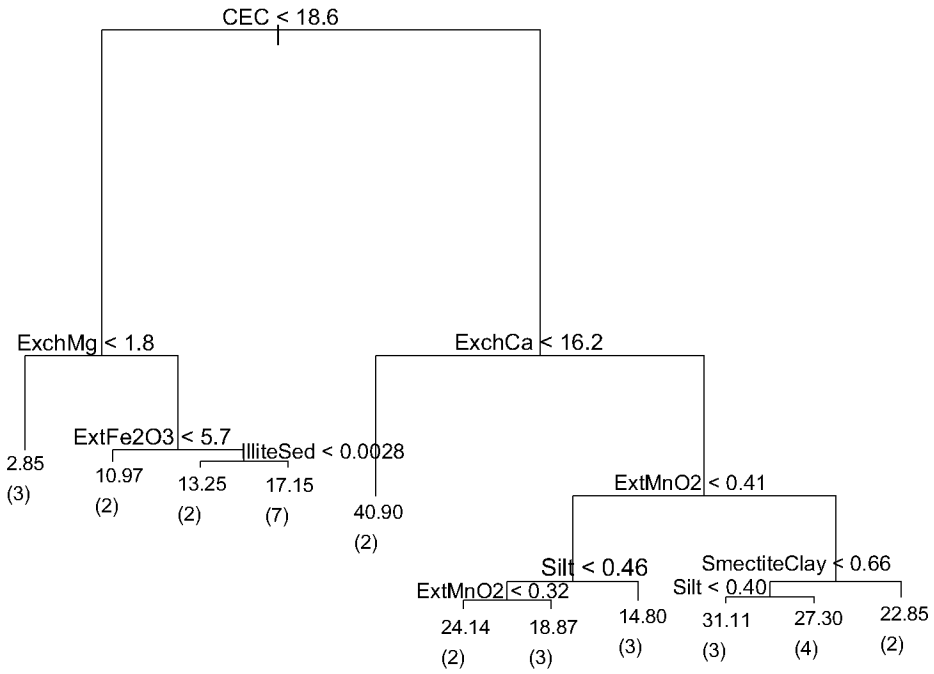

Figure 13. Regression tree for uranium K_d. Significant predictors are sum of exchangeable cations (CEC), exchangeable Mg (ExchMg), exchangeable Ca (ExchCa), extractable Fe_2O_3 (ExtFe2O3), illite fraction of sediment (IlliteSed), extractable MnO_2 (ExtMnO2), silt fraction (Silt), and smectite fraction of clay (SmectiteClay). Predicted uranium K_d is given at nodes with number of observations per category in parentheses. Length of vertical line below node represents importance of that predictor.

The regression trees result in better model fit statistics than the polynomial regressions (see Table 10). The residuals are smaller for the regression trees, correlations higher, and residuals more believably normal. This is not surprising considering the regression trees used more predictors. While K_d values can be predicted from measurements of material properties, measurement of several properties is necessary to achieve predictions that approach the measured values. Consequently this comparison does not show that a single or a few measurements of material properties, instead of directly measuring K_d values, would provide an easier or cheaper approach to determining retardation in interbed sediments.

3.4 Spatial Distribution

Kriging does not require distributional assumptions, but does assume the variable to have a symmetric distribution. The highly skewed neptunium K_d and log-transformed data were modeled and the predictions compared. The kriging predictions on the log-transformed data were back-transformed using a simple exponential. The uranium K_d values were assumed normally distributed. The variogram models were determined by separately examining variogram clouds and empirical variograms by interbed for both raw and log-transformed neptunium K_d and uranium K_d.

The neptunium K_d variogram cloud for the C-D interbed (see Figure 14) support the range between 200 and 400 m, while the variogram cloud for the B-C interbed (see Figure 15) supports no value for the range. Based on previous work (Leecaster 2002) and the variograms described below, the empirical variograms for both interbeds were modeled with a range of 305 m. The sill for both interbeds was estimated by eye to be 2,500 and the nugget to be zero (see Figures 16 and 17).

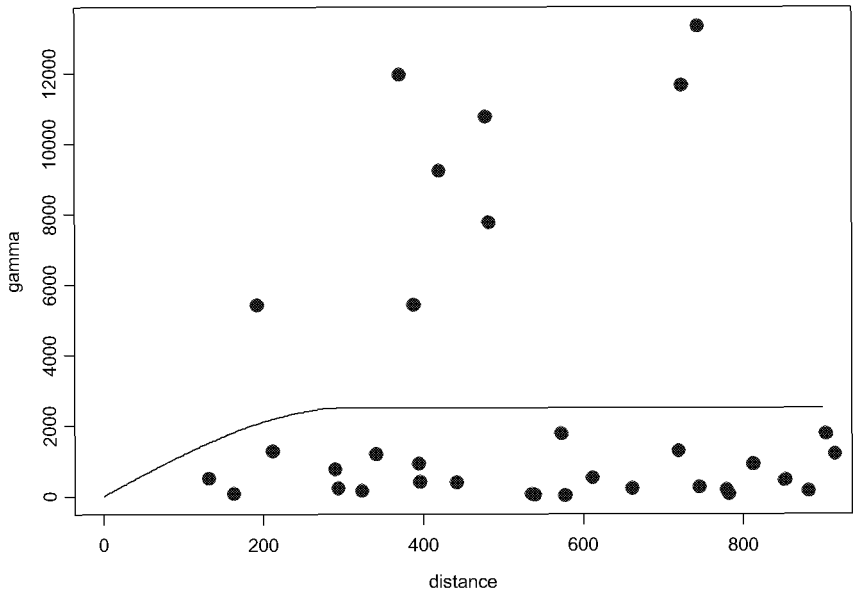

Figure 14. Variogram cloud for raw neptunium K_d from C-D interbed with spherical model (range = 305 m, nugget = 0, sill = 2500).

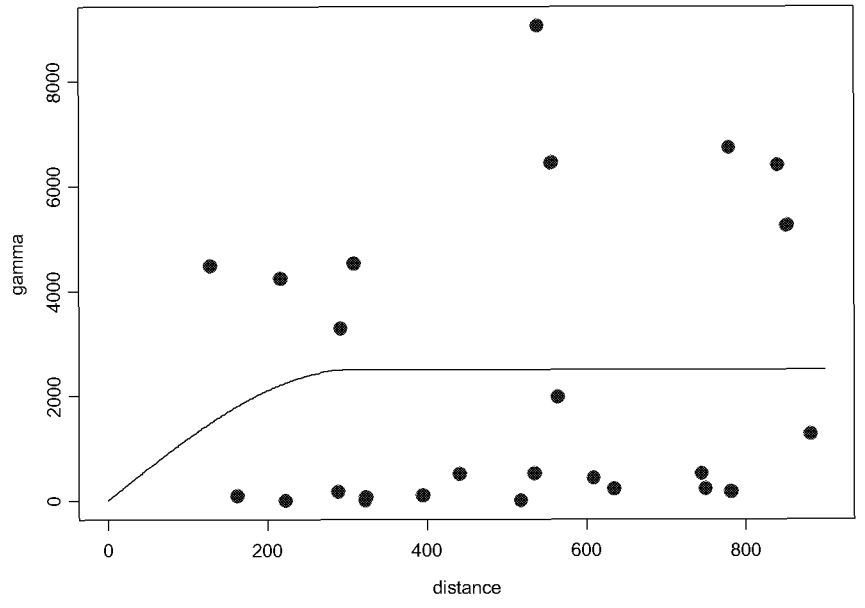

Figure 15. Variogram cloud for raw neptunium K_d from B-C interbed with spherical model (range = 305 m, nugget = 0, sill = 2500).

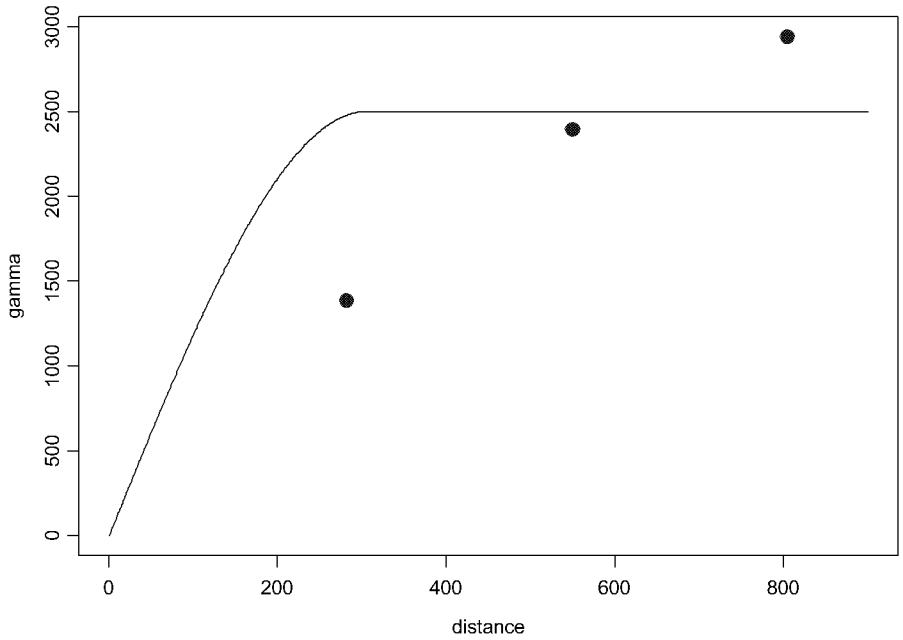

Figure 16. Empirical variogram for raw neptunium K_d from B-C interbed with spherical model (range = 305 m, nugget = 0, sill = 2500).

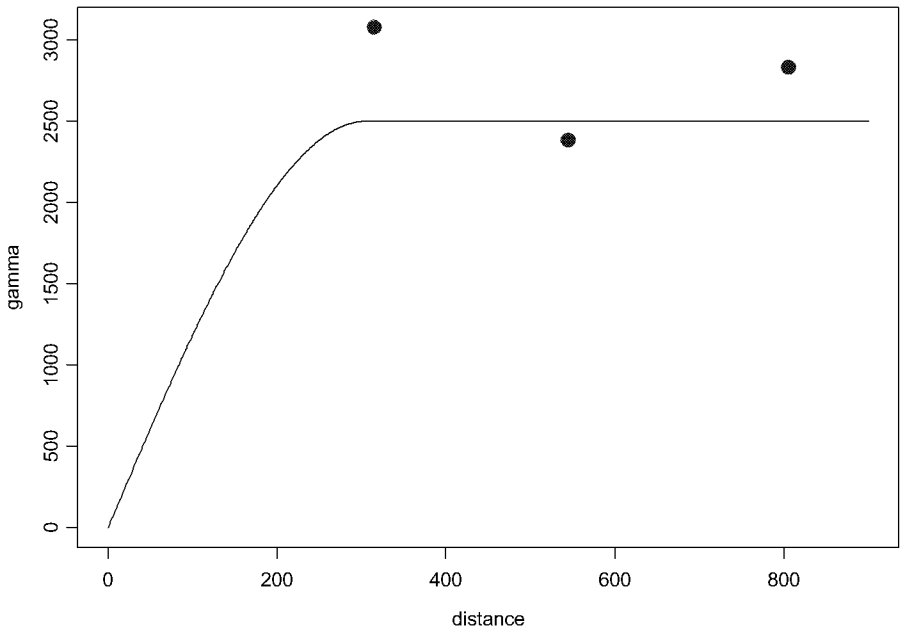

Figure 17. Empirical variogram for raw neptunium K_d from C-D interbed with spherical model (range = 305 m, nugget = 0, sill = 2500).

A nugget of zero implies there is no small-scale variability. There were two samples (i.e., O-5 and O-7 from the B-C interbed) with replicate analyses. These resulted in standard deviations of 0.7 for uranium K_d and 0.04 for log neptunium K_d. The standard deviations are very small compared to the variances between pairs of samples, so the assumption of zero nuggets is not unrealistic.

The log neptunium K_d variogram clouds for the C-D interbed (see Figure 18) support a range of about 305 m, while the variogram cloud for the B-C interbed (see Figure 19) supports no value for the range. The empirical variograms for both interbeds were modeled by a spherical variogram with a range of 305 m. The different sills for the interbeds were estimated by eye based on the empirical variograms for the interbeds separately, although there are little data. The variogram for the log of neptunium K_d values for the B-C interbed (see Figure 20) was modeled by a spherical model with a range = 305 m, sill = 1.2, and nugget = 0. The variogram for the C-D interbed (see Figure 21) was modeled by a spherical model with a range = 305 m, sill = 3, and nugget = 0.

The uranium K_d variogram cloud from the B-C interbed (see Figure 22) does not show a distinct range. The one large semi-variance at lag 152.4 m is large and without that pair a range between 305 and 457.2 m is supported. The uranium K_d variogram cloud from the C-D interbed (see Figure 23) does support a range between 305 and 457.2 m. The empirical variograms are very limited by the number of pairs used to estimate, but do provide an estimate of the sill. The uranium K_d variogram for the B-C interbed (see Figure 24) was modeled by a spherical model with a range = 305 m, sill = 50, and nugget = 0. The variogram for the C-D interbed (see Figure 25) was modeled by a spherical model with a range = 305 m, sill = 150, and nugget = 0.

The spatial correlation range for uranium and neptunium K_d match the spatial correlation range of porosity from the SDA (Leecaster 2002). That study was based on 112 samples analyzed for porosity and permeability from 32 surface locations, 52 within the B-C interbed and 60 within the C-D interbed. Although the variogram for permeability was pure nugget (i.e., no evidence of spatial correlation), the variogram range for porosity in both interbeds was 305 m, equal to the variogram range for the K_d values. The variogram parameters do affect the kriging predictions, but there is a degree of robustness to their specification. If the estimated variogram model is compatible with the true variogram (i.e., similar to the true variogram at close distances), then the kriging predictions are asymptotically accurate and precise (Stein 1988). This does not negate the effect distance between sites as with the kriging variance, which increases with increasing distance among sites.

The uranium K_d, neptunium K_d, or log of neptunium K_d for both interbeds was not significantly related to direction (easting or northing) based on linear regressions (p-values > 0.05). Thus, ordinary kriging could be used and local stationarity assumed. This also indicates that there are no facility-wide trends in the sorption characteristics of interbeds.

The predictions made on log-transformed neptunium K_d were back-transformed in two ways (Gilbert 1987). The simple exponential back-transformation is negatively biased for the mean of lognormal data, but is unbiased for the median of lognormal data. The unbiased back-transformation for the mean that is generally recommended adds a fraction of the variance prior to exponentiation. For kriging predictions, this bias correction term is one half the difference between the variance of the log data and the variance of the log-scale predictions. Due to the limited number of sample locations, the prediction variance is quite large, causing the predictions to be large as well. Although, this back-transformation is unbiased for truly lognormal data, the neptunium K_d data have not been shown to be lognormal. Both the median and the mean may be reasonable statistics, but the median is more conservative (i.e., the predicted neptunium K_d values are lower) and may be more realistic given the lack

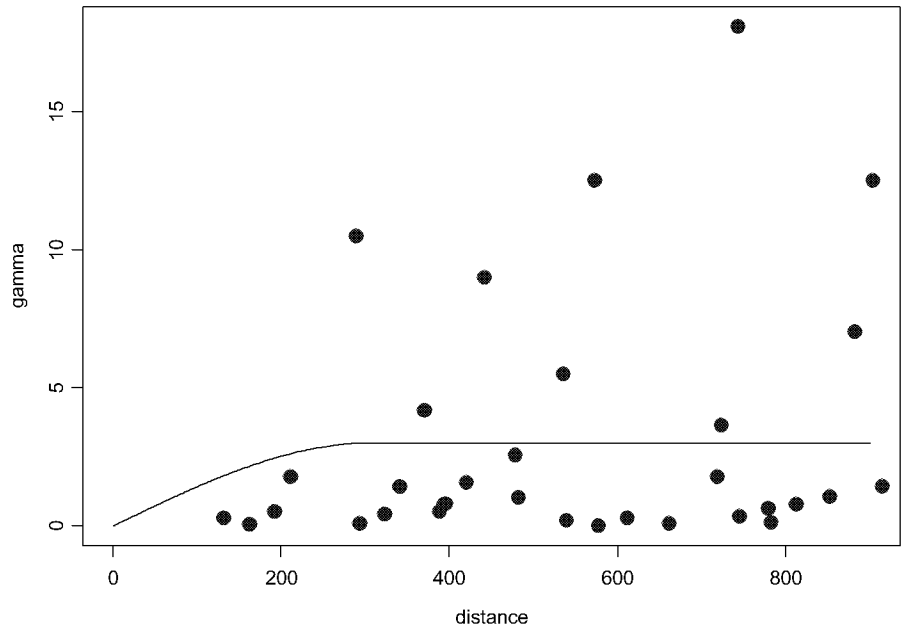

Figure 18. Variogram cloud for log transformed neptunium K_d from the C-D interbed with spherical model (range = 305 m, nugget = 0, sill = 3).

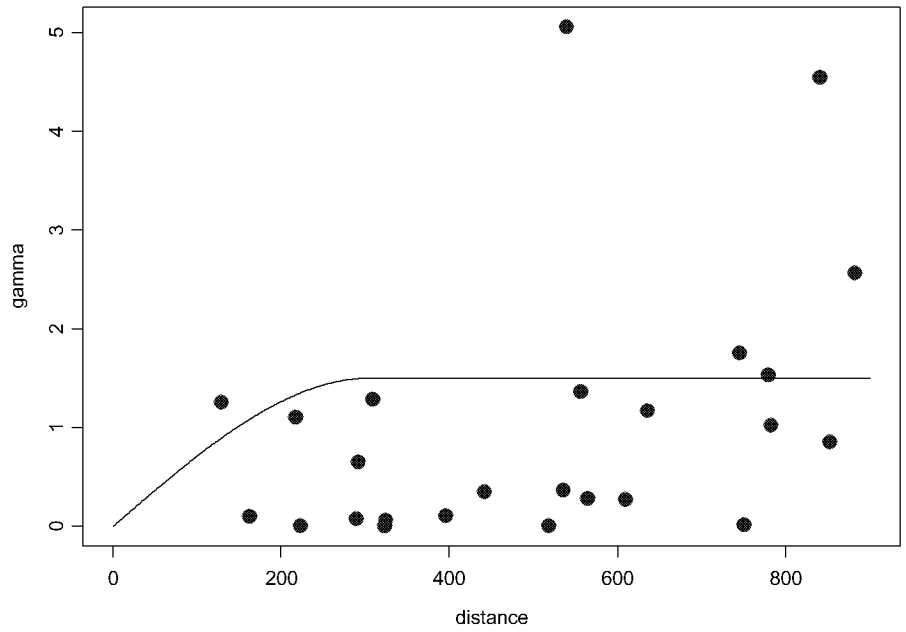

Figure 19. Variogram cloud for log transformed neptunium K_d from the B-C interbed with spherical model (range = 305 m, nugget = 0, sill = 1.5).

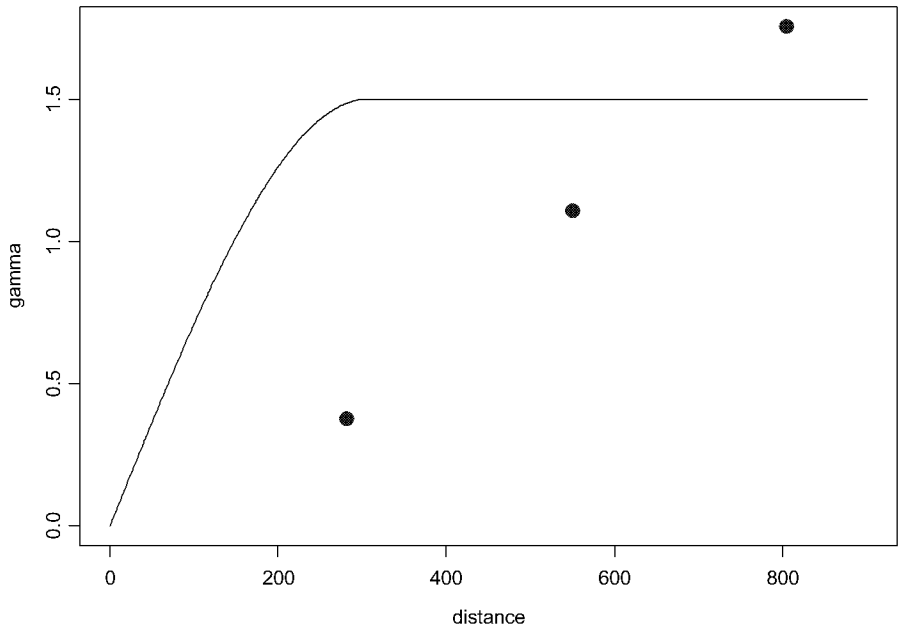

Figure 20. Empirical variogram for log transformed neptunium K_d from the B-C interbed with spherical model (range = 305 m, nugget = 0, sill = 1.5).

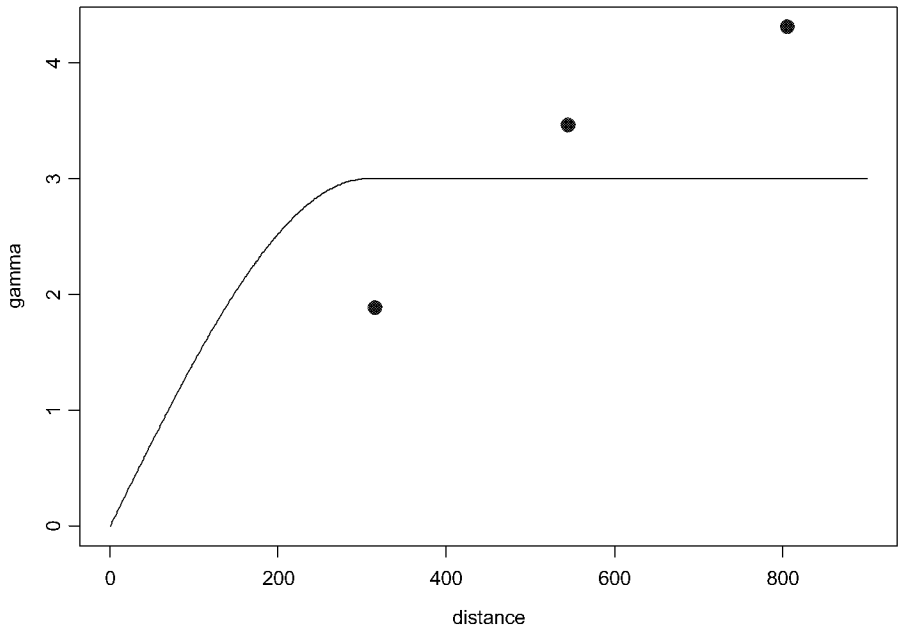

Figure 21. Empirical variogram for log transformed neptunium K_d from the C-D interbed with spherical model (range = 305 m, nugget = 0, sill = 3).

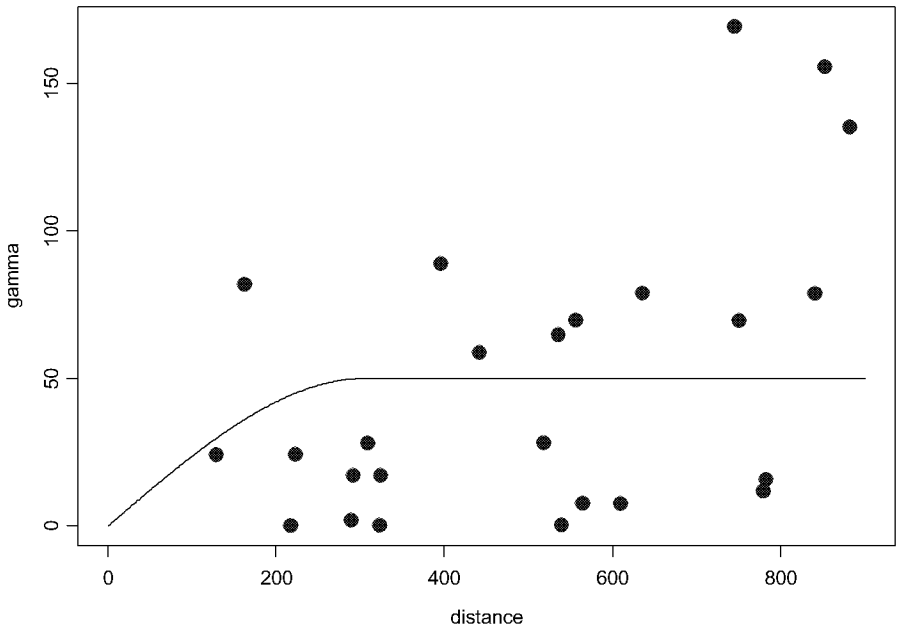

Figure 22. Variogram cloud for uranium K_d from the B-C interbed with spherical model (range = 305 m, nugget = 0, sill = 50).

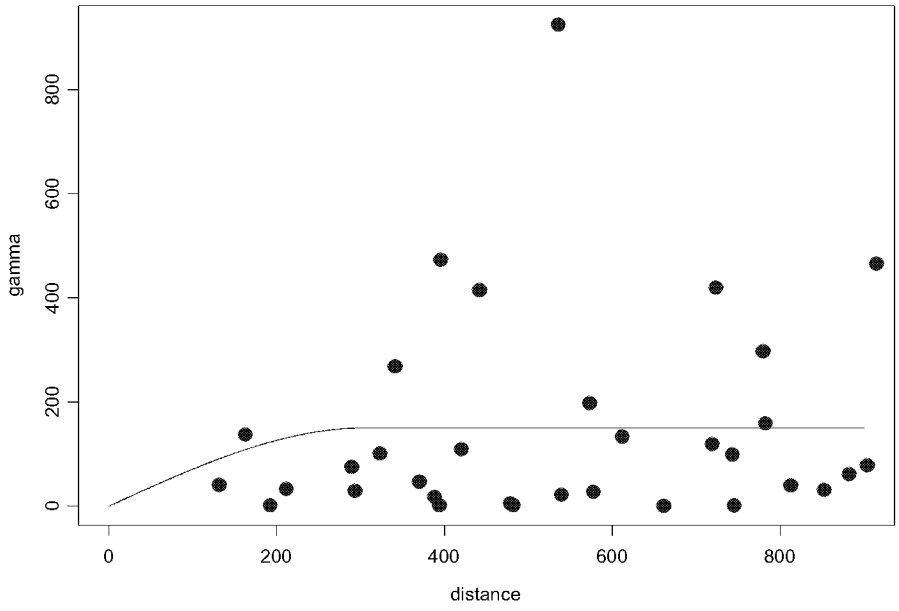

Figure 23. Variogram cloud for uranium K_d from the C-D interbed with spherical model (range = 305 m, nugget = 0, sill = 150).

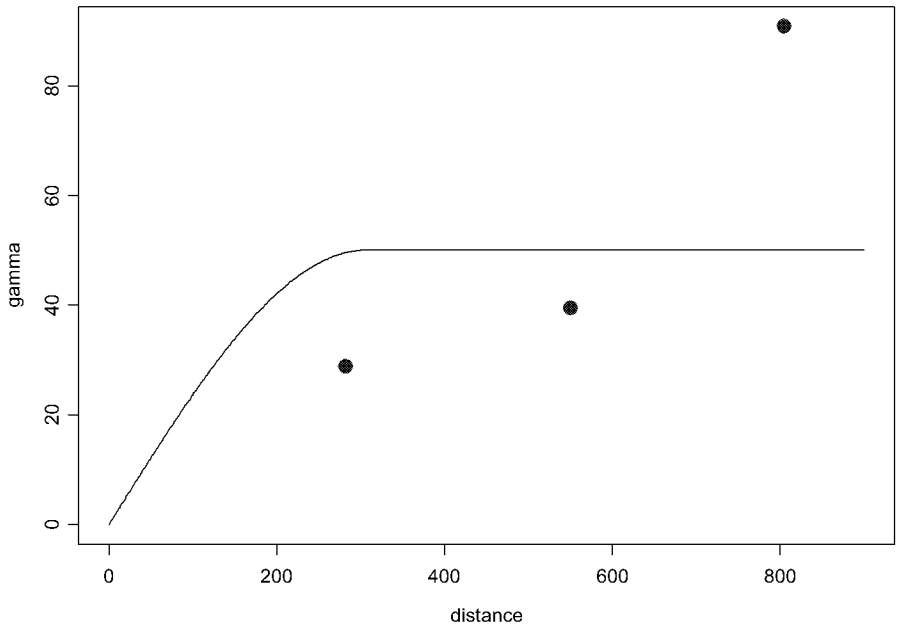

Figure 24. Empirical variogram for uranium K_d from the B-C interbed with spherical model (range = 305 m, nugget = 0, sill = 50).

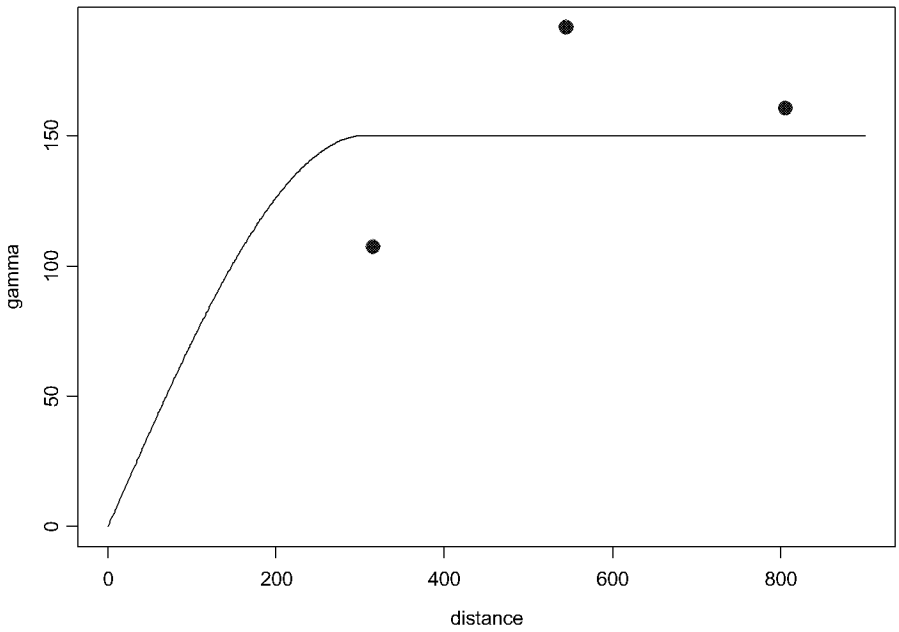

Figure 25. Empirical variogram for uranium K_d from the C-D interbed with spherical model (range = 305 m, nugget = 0, sill = 150).

of support for a truly lognormal distribution. Thus, only raw data predictions and simple, back-transformed predictions are presented; the transformed data analysis provides the more conservative (i.e., smaller) predictions.

The predicted distribution of neptunium K_d in the B-C interbed from using transformed data is shown in Figure 26 with kriging standard errors shown in Figure 27. These standard errors were simply exponential back-transformed and are biased low. The predicted distribution of neptunium K_d in the B-C interbed from raw data is shown in Figure 28 with kriging standard errors shown in Figure 29. Predictions outside the range of sample locations become constant due to lack of additional sample data to influence the prediction. This constant value is considered the predicted background level for the K_d. The background K_d value for the area surrounding the SDA for this interbed is predicted to be 35 mL/g using the transformed data, and 51 mL/g using the raw data. Otherwise for both sets of predictions, there are some very high and very low spots in the K_d surface, but these are not correlated to other nearby measurements and result in bulls eye patterns. The overall picture for neptunium sorption in the B-C interbed is a fairly uniform retardation potential with one spot to the south of the SDA boundary with low retardation at well O-2. However, even the low K_d measured in well O-2 is higher than the K_d value of 8 mL/g used in previous risk assessment calculations.

The predicted distribution of neptunium K_d in the C-D interbed from using transformed data is shown in Figure 30 with kriging standard errors shown in Figure 31. These standard errors were simply exponential back-transformed and are biased low. The predicted distribution of neptunium K_d in the C-D interbed from raw data is shown in Figure 32 with kriging standard errors shown in Figure 33. The background neptunium K_d value for the C-D interbed is predicted to be 18 mL/g using the transformed data, and 39 mL/g using the raw data. Within the SDA, the measured K_d values are higher, with two for transformed data and three for raw data, elevated K_d values giving a region with sorption coefficients exceeding 40 mL/g. While the difference in background concentrations between the B-C and C-D interbeds appears large (i.e., 35 and 18 mL/g for transformed data and 51 and 39 mL/g for raw data), the difference between the interbeds is not statistically significant because there is a very large variance in the measured neptunium K_d values. Overall, the neptunium K_d value of 8 mL/g used in risk and performance assessment models is much smaller than all but a few measured values from the SDA, and is smaller than the spatially predicted K_d values for all but a few nodes in the computer model, outside the boundary of the SDA. The smallest K_d values are predicted at well O-2 in the B-C interbed and at well O-7 in the C-D interbed.

The predicted distribution of uranium K_d in the B-C interbed is shown in Figure 34 with kriging standard errors shown in Figure 35. In the B-C interbed, predicted uranium sorption coefficients are fairly uniformly distributed near 19 mL/g with a few slightly lower and a few slightly higher values. The areas of elevated and decreased sorption appear as bull's eyes on the map, indicating little spatial correlation at the scale of the measurements.

The predicted distribution of uranium K_d in the C-D interbed is shown in Figure 36 with kriging standard errors shown in Figure 37. The predicted background value of uranium sorption in the C-D interbed is similar to the B-C interbed at 20 mL/g. There are some small variations about this value with an area just north of the SDA boundary at well O-03, and a second area to the southwest of the SDA at well O-07 having K_d values closer to 10 mL/g. The uranium K_d value of 6 mL/g used in the risk and performance assessment models is much smaller than all but three of the measured values. Only the predicted value for the nodes around well O-7 in the C-D interbed are as low as the current K_d value used in the risk assessment.

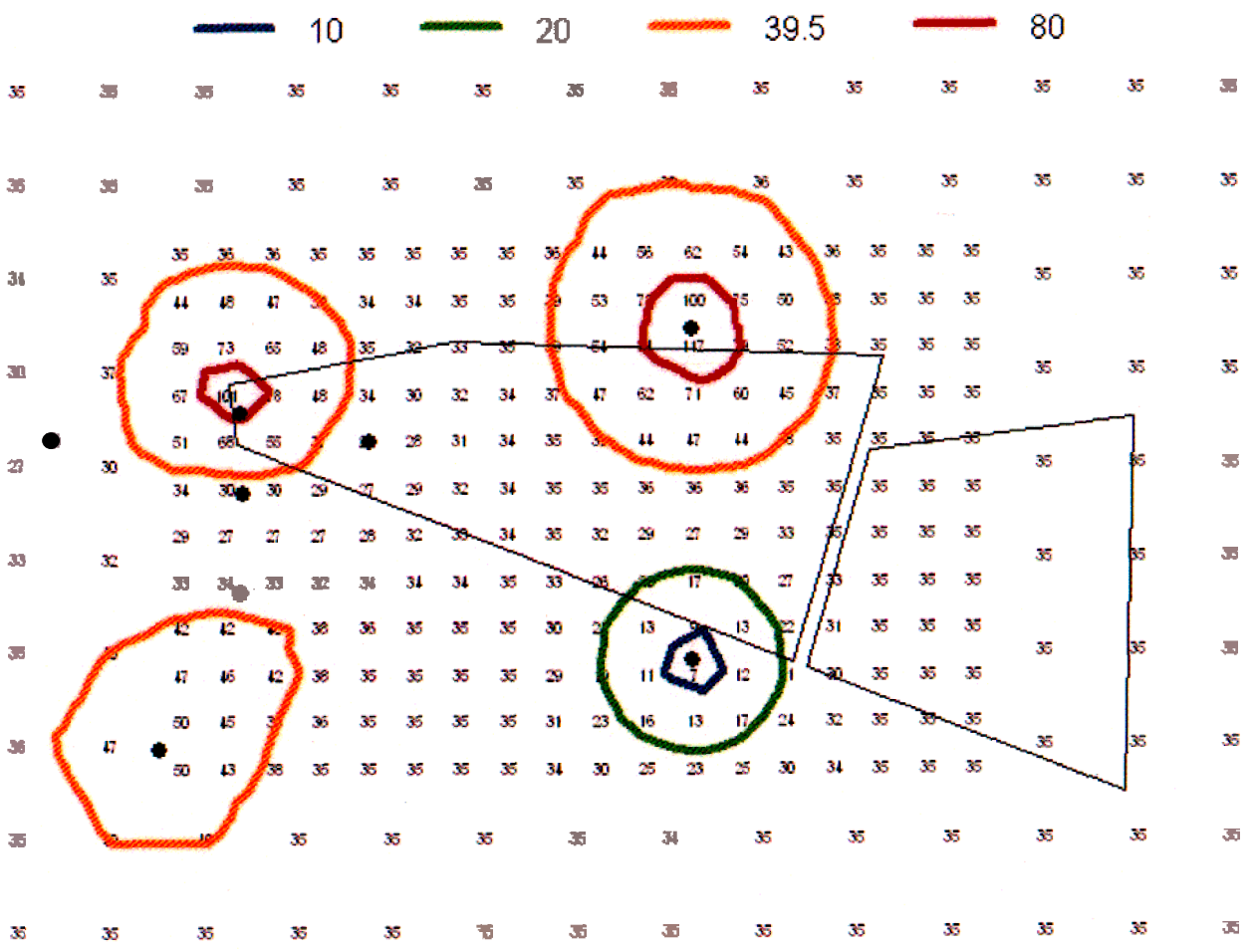

Figure 26. Predicted neptunium K_d from transformed data for B-C interbed.

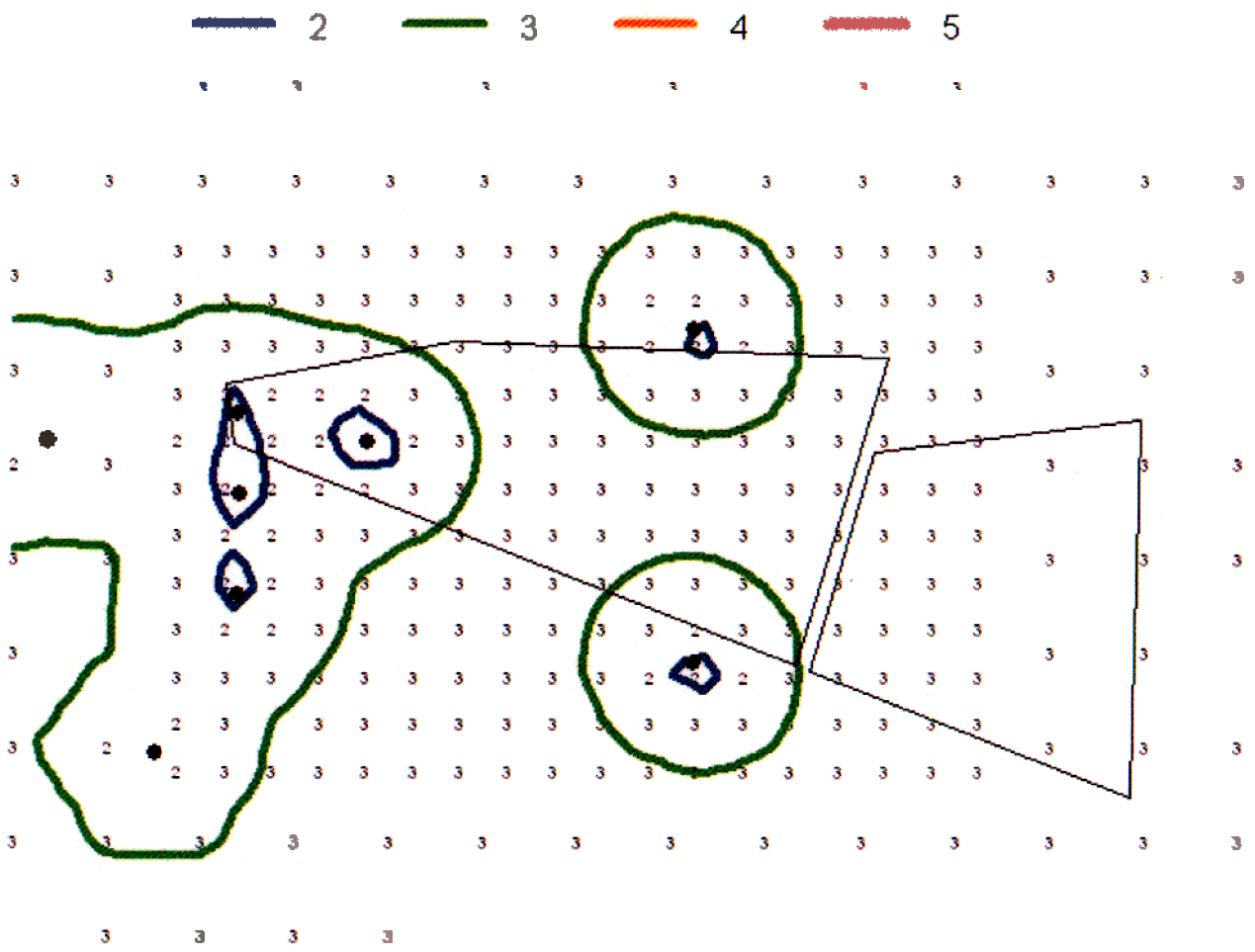

Figure 27. Standard errors for predicted neptunium K_d from transformed data for B-C interbed.

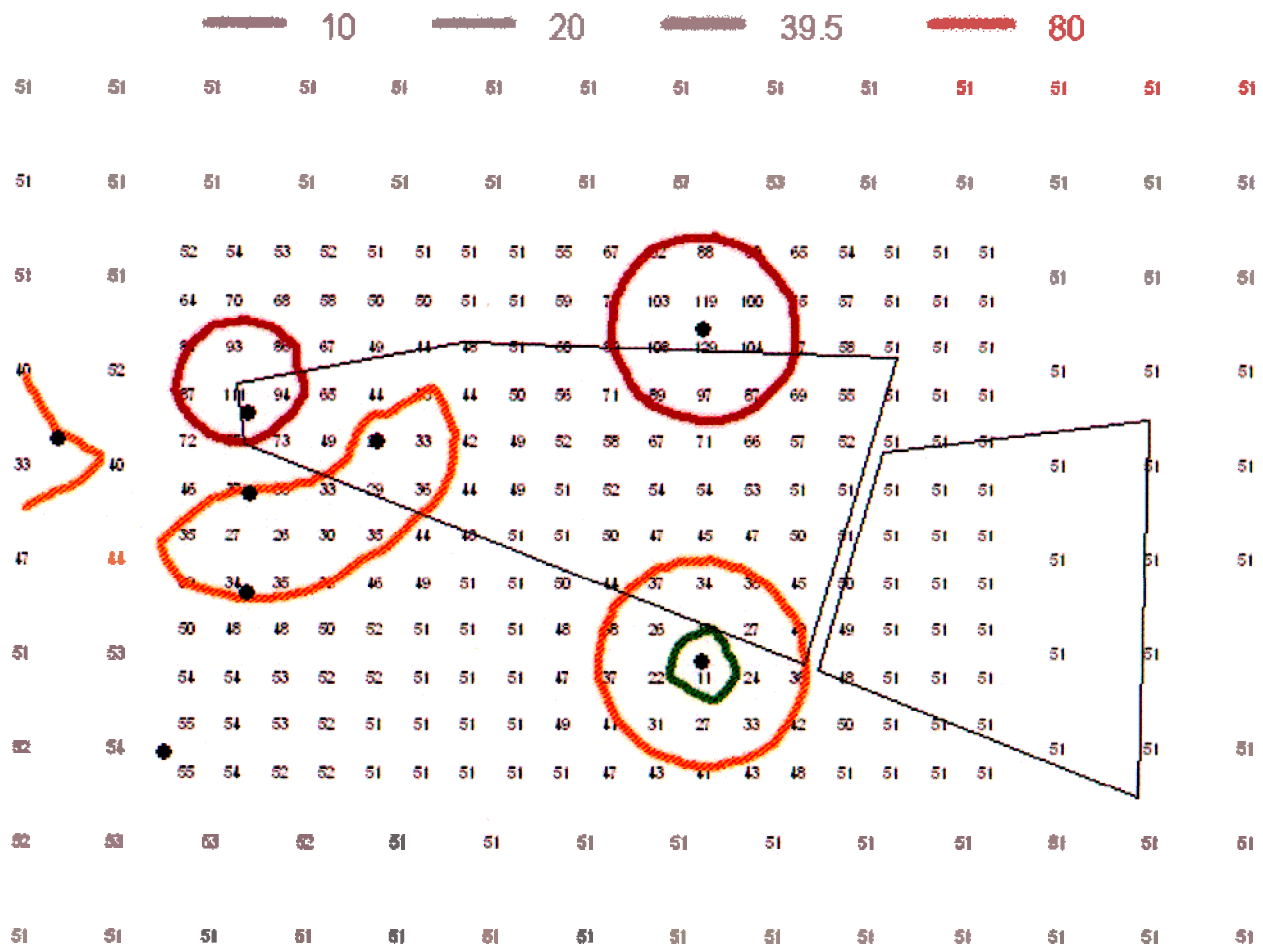

Figure 28. Predicted neptunium K_d from raw data for B-C interbed.

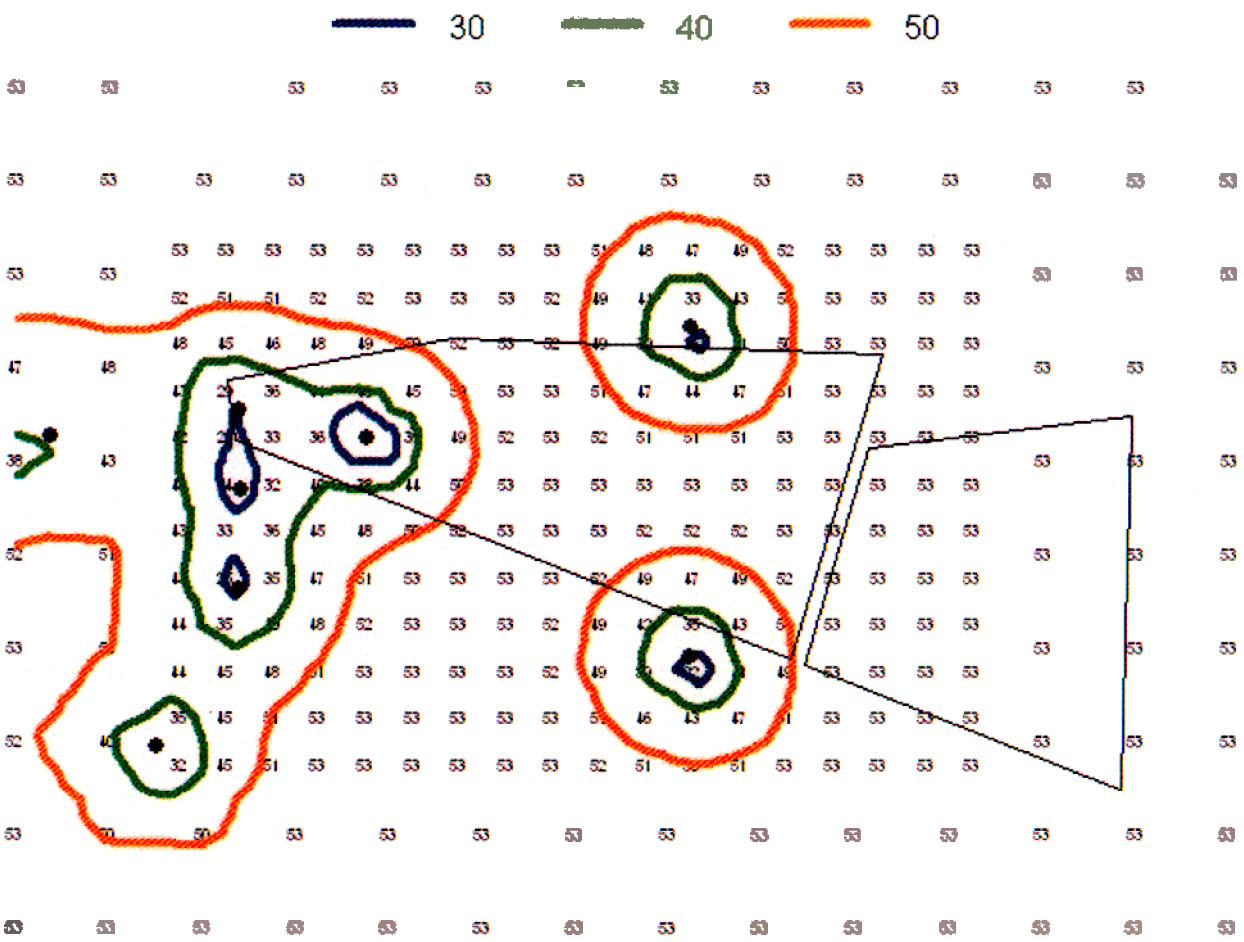

Figure 29. Standard errors for predicted neptunium K_d from raw data for B-C interbed.

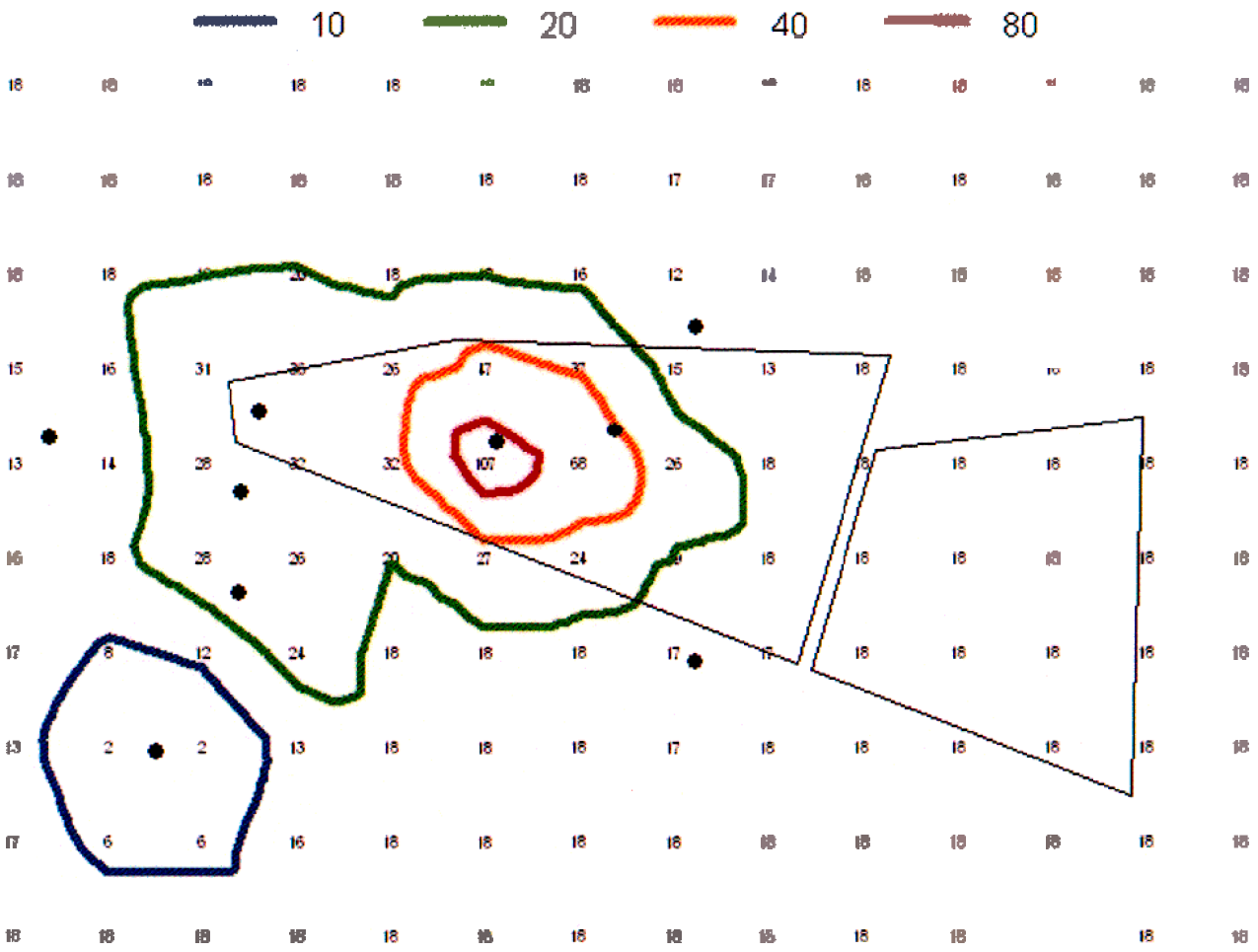

Figure 30. Predicted neptunium K_d from transformed data for C-D interbed.

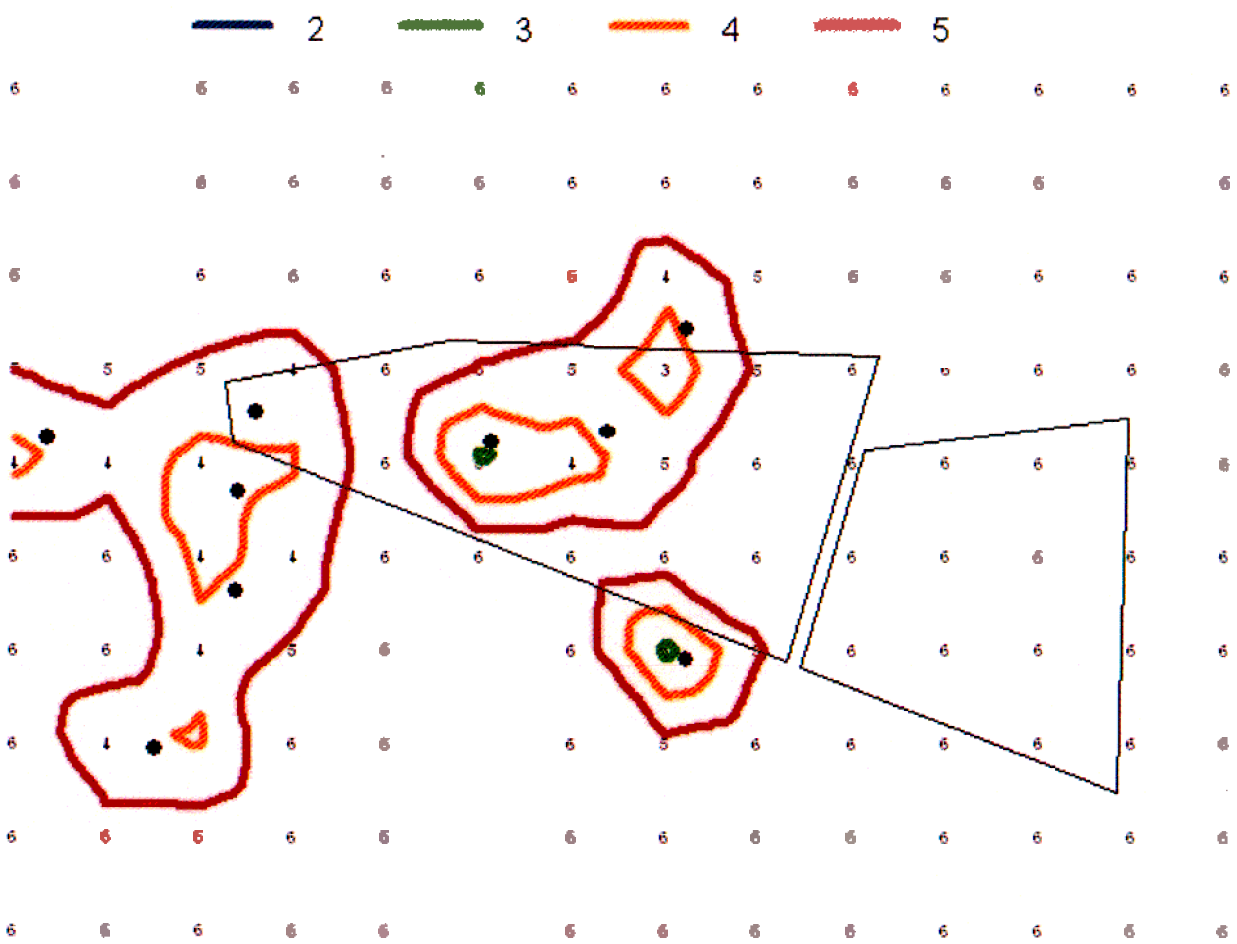

Figure 31. Standard errors for predicted neptunium K_d from transformed data for C-D interbed.

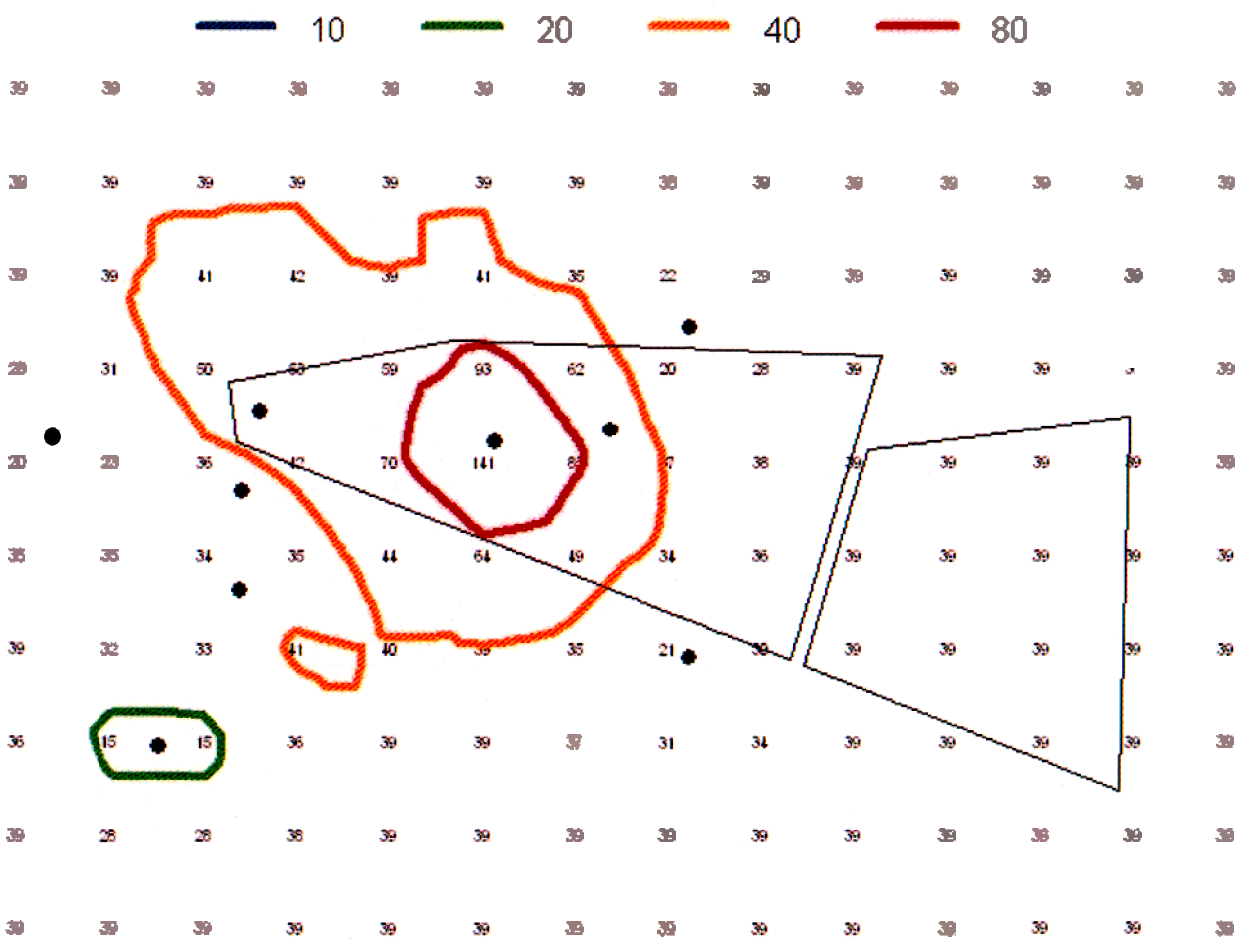

Figure 32. Predicted neptunium K_d from raw data for C-D interbed.

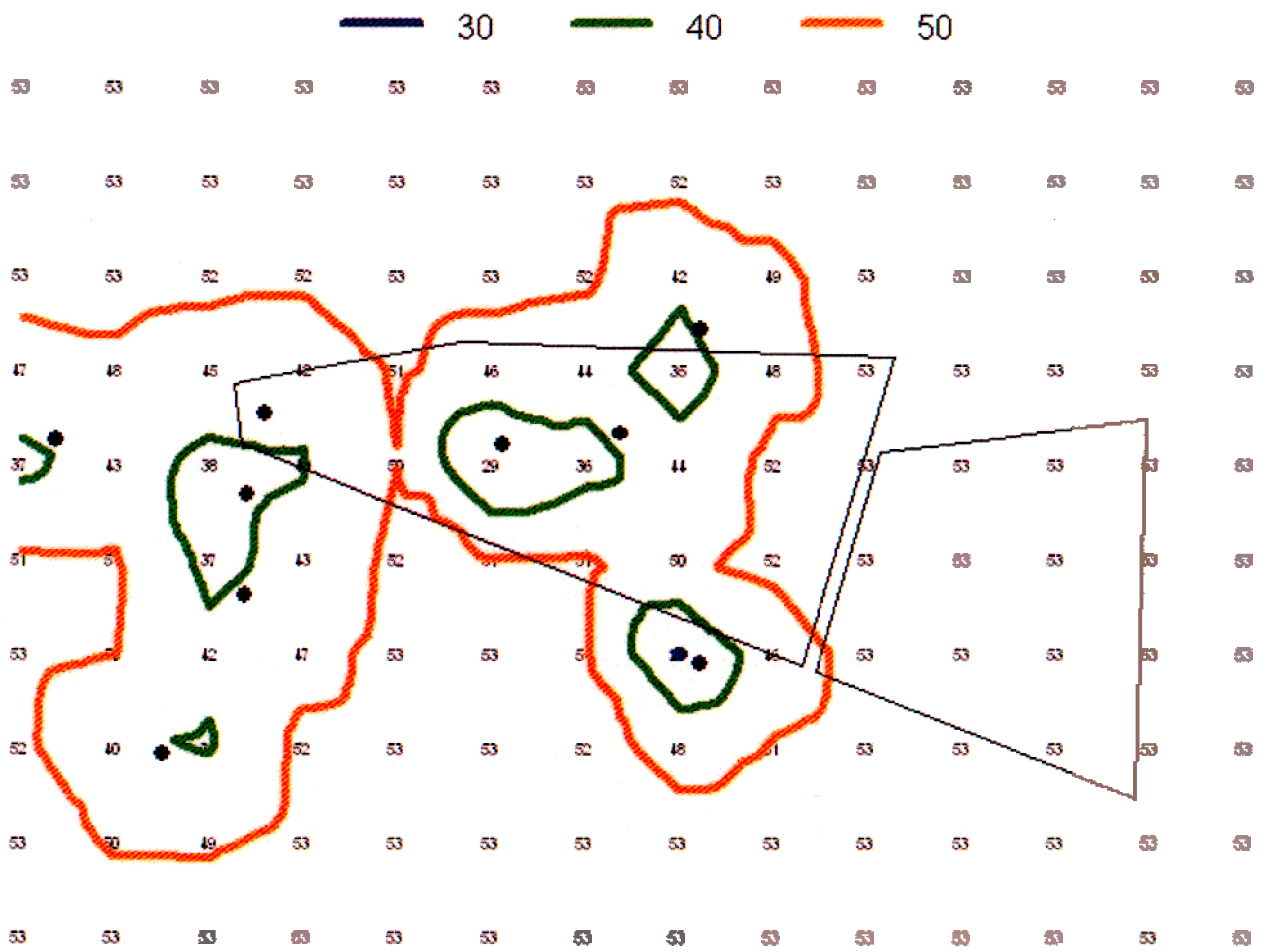

Figure 33. Standard errors for predicted neptunium K_d from raw data for C-D interbed.

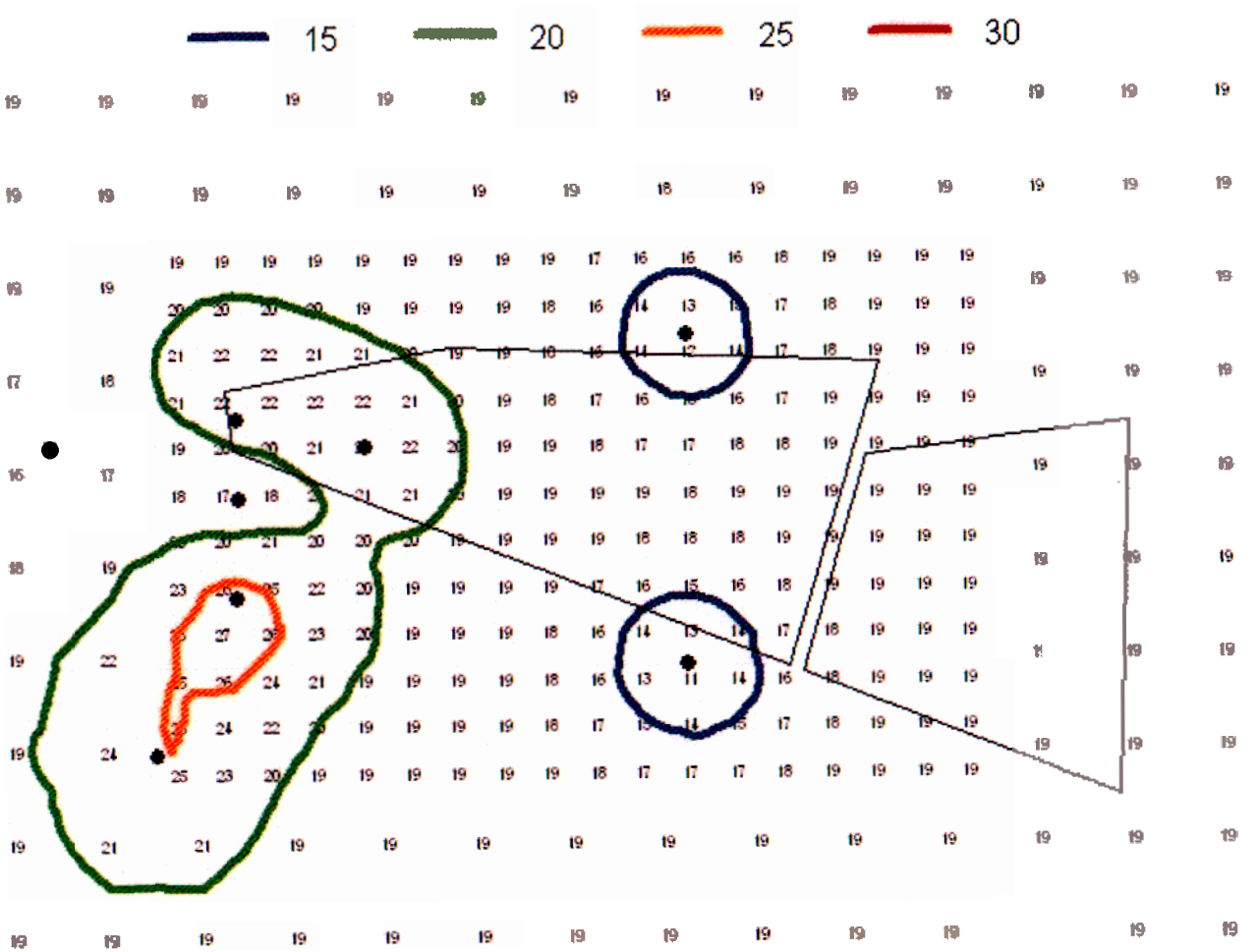

Figure 34. Predicted uranium K_d for B-C interbed.

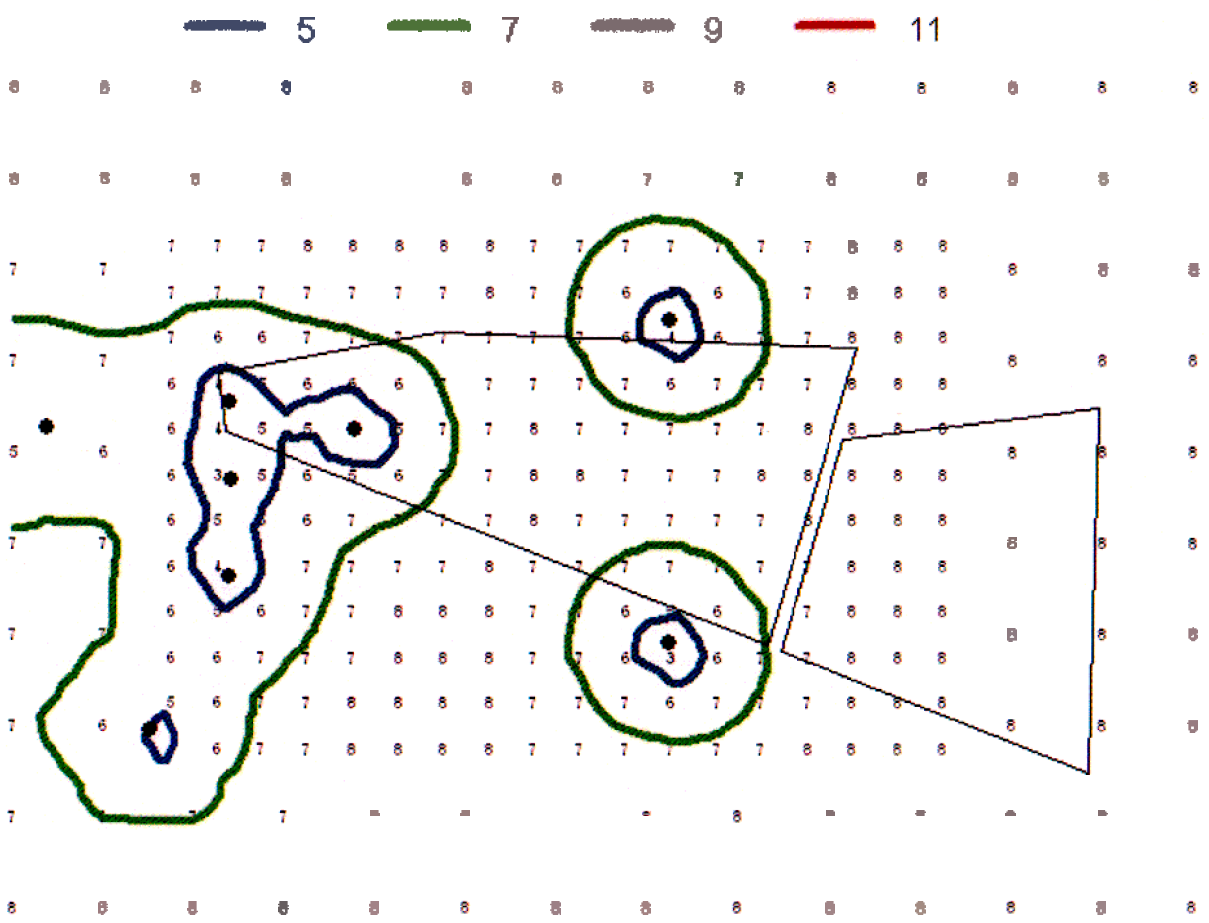

Figure 35. Standard errors for predicted uranium K_d for B-C interbed.

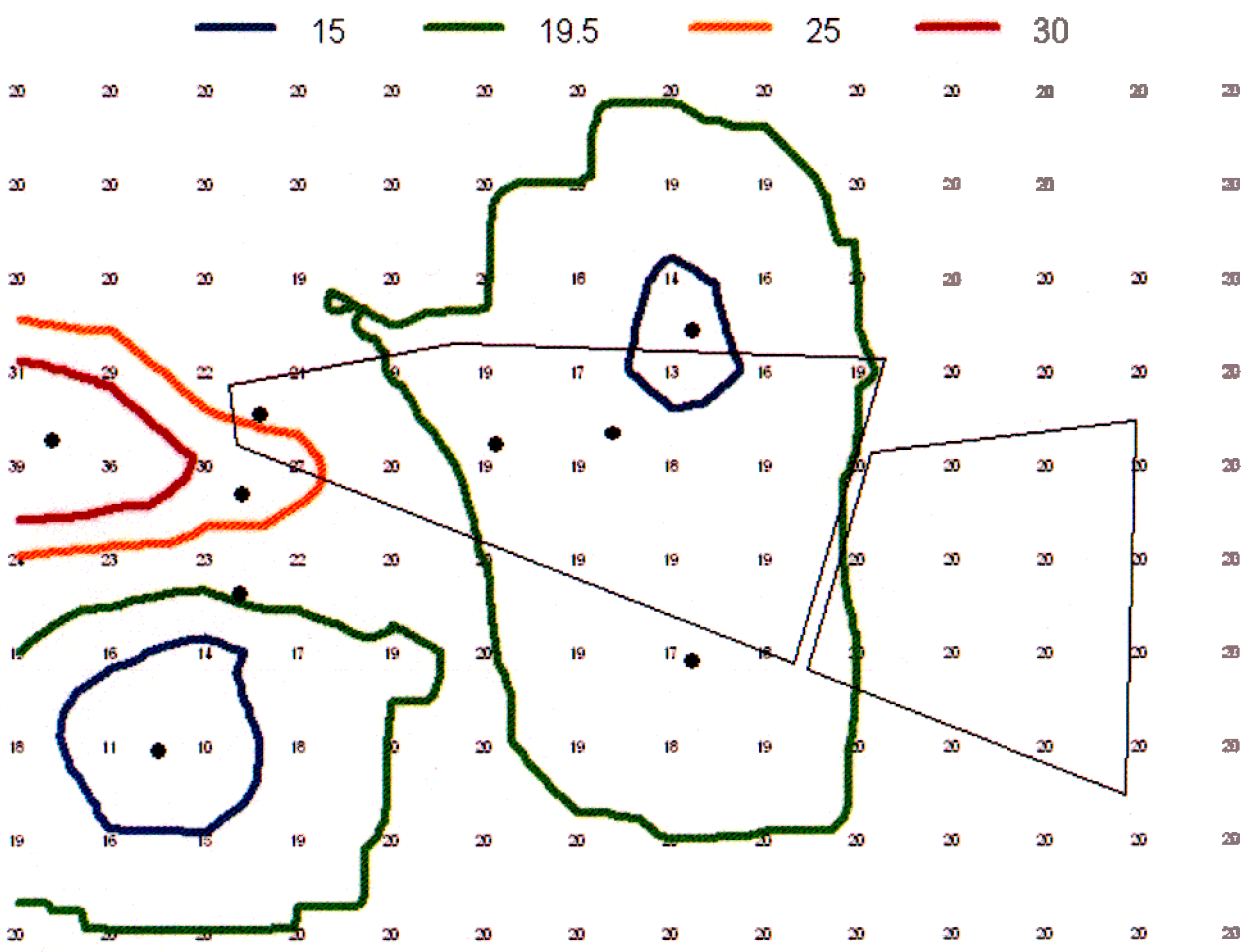

Figure 36. Predicted uranium K_d for C-D interbed.

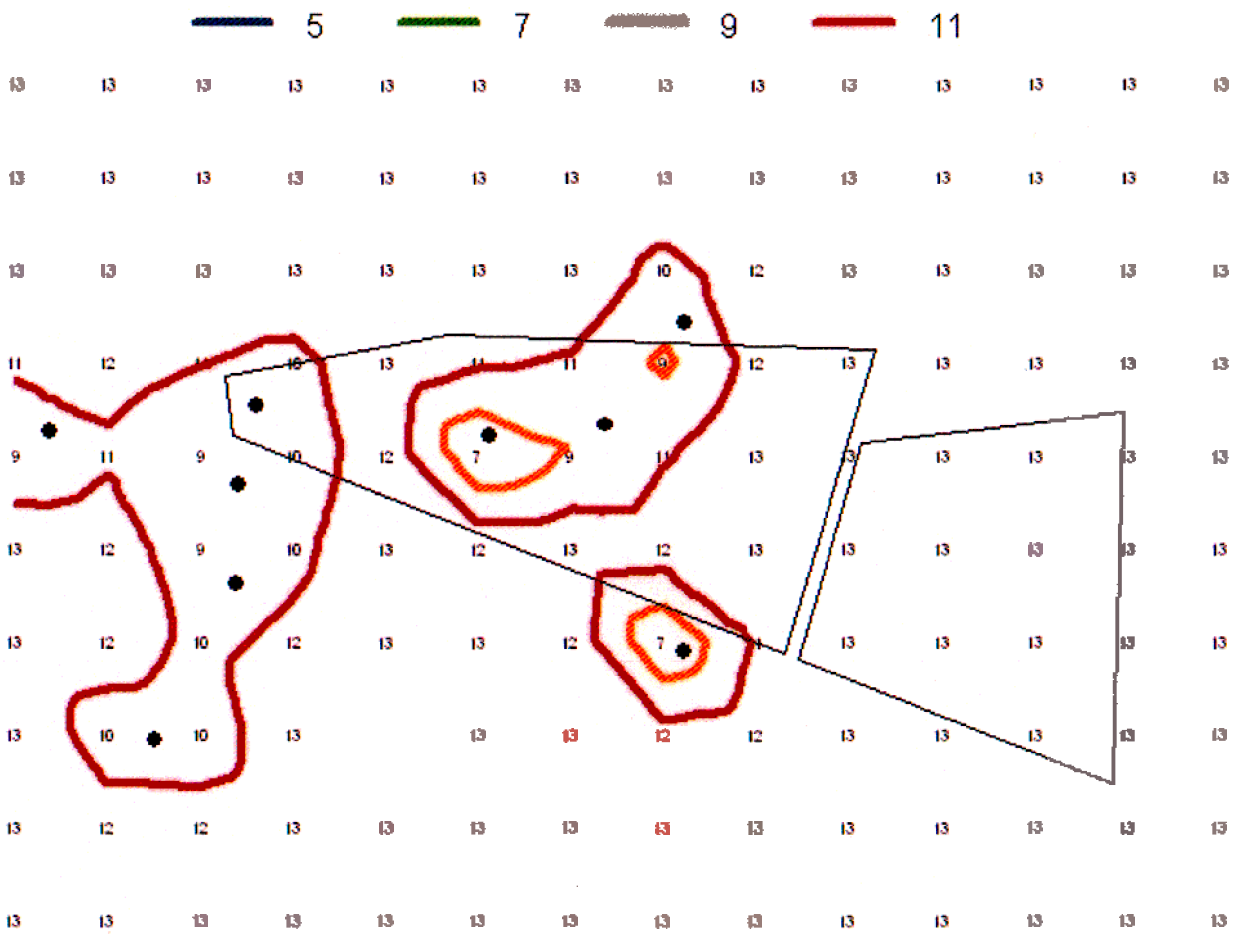

Figure 37. Standard errors for predicted uranium K_d for C-D interbed.

The maps of kriging standard errors display the increasing uncertainty with increasing distance from sample locations (Figures 27, 29, 31, 33, 35, and 37). The gradient of that change is related to the nugget, sill, and range of the estimated variogram. The standard errors for the neptunium K_d predictions from transformed data are underestimated by using the simple exponential back-transformation.

4. CONCLUSIONS

The K_d sample values are similar by depth and across the two interbeds for neptunium but not for uranium (see Figures 8 and 9). The difference between the interbeds for uranium K_d does not support the practice of assigning values to the sediments under the SDA without regard to placement among the basalt layers. The sample data do not support the hypothesis that fast-flow zones occur across interbeds, because the K_d correlations between interbeds are not significant.

The K_d values measured for neptunium and uranium at the SDA are not strongly related to any one covariate that was measured, and so simple parametric predictive models for uranium and neptunium sorption do not appear to be viable. Although the predictions from the tree models are promising, measurement of multiple indicators is just as expensive as measuring K_d and not as accurate. From correlations among the K_d values and material properties, sorption of uranium and neptunium are primarily related to the presence of clay minerals, with some sorption related to extractable iron minerals.

There are no significant differences in K_d values among wells for either uranium or neptunium, but there is evidence of spatial correlation. Therefore, although the results are correlated spatially, there are no large differences spatially. The spatially varying predictions made for neptunium K_d and uranium K_d are the best estimates given the data. This is one of few cases where K_d values were measured on a spatial scale that allowed spatial modeling. Generally, one K_d value is used to represent a large area without regard to spatial heterogeneity. The neptunium K_d values obtained from the literature for Hanford (Kaplan and Serne 1995; Kaplan et al. 1995) are 2.4 to 29.1 mL/g, and for uranium are 0.08 to 79.3 mL/g (although all but one result are less than 2.3 mL/g). Neptunium K_d values from the INEEL SDA range from 0.1 to 250.6 mL/g with a median of 35.3 mL/g and, for uranium, range from 3 to 54.5 mL/g with a median of 20.4 mL/g. The median of the kriging predicted values is 34.7 mL/g for neptunium in the B-C interbed, 17.8 mL/g for neptunium in the C-D interbed, 18.8 mL/g for uranium in the B-C interbed, and 19.6 mL/g for uranium in the C-D interbed.

The kriging predictions are limited by the sample data and the variogram model. Limited sample data provide less confidence in the estimated variogram model, especially if there is limited data at short distances to estimate the variogram range. Although misspecification of the variogram, if the model is consistent (i.e, similar to the true variogram at close distances), may not overly influence the predictions (Stein 1988), the variance of the kriging predictions depends on the sample locations. In our case, the data are limited and some sample locations are far from others. Thus, the precision of the predictions is generally low, and is especially low beyond the sample data locations that are included in the prediction grid.

The predictions are close to the median sample values, except for the neptunium K_d predictions from the raw data, which might support using a single K_d value for risk assessment models. The average difference between the spatial prediction and the median for the interbed is 10 mL/g for transformed neptunium from B-C, 6 mL/g for transformed neptunium from C-D, 26 mL/g for neptunium from B-C, 15 mL/g for neptunium from C-D, 2.3 mL/g for uranium from B-C, and 2.3 mL/g for uranium from C-D. The large differences for the untransformed neptunium predictions are a result of comparing to the median versus the mean, which is almost twice as large. The other differences in predictions may come from a few extreme sample values that influence their surrounding predictions. This is seen in the neptunium K_d values for the B-C versus C-D interbeds. The B-C interbed has much higher predictions

overall, but the sample data results do not differ by interbed. The much higher predictions for B-C and lower predictions for C-D overall are due to a having two high values in the B-C interbed that are located on the spatial edge of the data, and influence outlying area predictions. There is one high value for the C-D interbed, but it is not on the edge of the sample data locations; therefore, the nearby lower values restrict its influence upon outlying areas. These three high neptunium K_d values were from different surface locations. Therefore, the high values did not occur in a single interbed, nor were they restricted spatially. The neptunium K_d values may be lognormal, thus allowing for the few very high sample results while maintaining a moderate median value. These high values could represent pockets of sediment with much greater retardation capability. This could be determined through additional sampling efforts.

Although a single value may be sufficient, the K_d results from this study do not support the assumed values that were used in the groundwater risk model for this site. The assigned values are 8 mL/g for neptunium and 6 mL/g for uranium. These values are on the very low end of the distribution of values (see Table 8), and below the minimum uranium result for the B-C interbed. The assigned values are below the lower 95% confidence interval for the mean except for neptunium in the C-D interbed. These extremely small K_d values are not representative of the SDA. More appropriate values might be the medians at 26.9 mL/g for neptunium and 17.3 mL/g for uranium.

Additional samples could provide valuable information. If the risk assessment proves sensitive to spatially varying K_d values, then further sampling could be done to improve the precision of the predictions, as well as to investigate possible areas of high K_d values. Because there is evidence of spatial correlation within this small data set, more data could prove useful to determining spatially-specific predictions of K_d values for neptunium and uranium for the SDA. These could, in turn, improve the accuracy of a groundwater risk model. If groundwater risk assessments for the SDA are sensitive, then other studies may benefit from collecting multiple samples for K_d values from each site. The variograms from these twelve surface locations are not well constrained and models are applied with caution. More sample locations would provide greater confidence in the variogram model and therefore in predictions. The location of any extra samples should take into account proximity to other sample locations (more sample pairs within the variogram range are needed), direction to other samples (assuring isotropy can be properly investigated), and spatial range of samples (cover a large area to avoid extrapolation).

5. ACKNOWLEDGEMENTS

Funding for this research was provided by the DOE Office of Environmental Management under contract DE-AC07-99ID13727.

6. REFERENCES

Anderson, S. R. and B. D. Lewis, 1989, *Stratigraphy of the Unsaturated Zone at the Radioactive Waste Management Complex, Idaho National Engineering Laboratory, Idaho*, Water Resources Investigation Report 89-4065, DOE/ID-22080, U.S. Geological Survey, May 1989.

ASTM D 422, 1963, "Standard Test Method for Particle-Size Analysis of Soils," American Society for Testing and Materials.

ASTM D 4319, 1993, "Standard Test Method for Distribution Ratios by the Short-Term Batch Method," American Society for Testing and Materials.

Ayaz, B., J. T. Coates, A. W. Elzerman, R. A. Fjeld, H. E. Holder, J. L. Myers, and B. A. Powell, 2003, *Development of Adsorption Parameters to Assess the Migration Potential for Uranium and Neptunium in the Subsurface at the INEEL*, INEEL/EXT-03-00306, Department of Environmental Science and Engineering, Clemson University, Idaho National Engineering and Environmental Laboratory, April 2003.

Bargar, J. R., R. Reitmeyer, and J. A. Davis, 1999, "Spectroscopic Confirmation of Uranium(VI)-Carbonato Adsorption Complexes on Hematite," *Environmental Science & Technology*, Vol. 33 (14), 2481-2484.

Barnett, M. O., P. M. Jardine, and S. C. Brooks, 2002, "U(VI) Adsorption to Heterogeneous Subsurface Media: Application of a Surface Complexation Model," *Environmental Science & Technology*, Vol. 36 (5), 937-942.

Bartholomay, R. C., 1990, *Mineralogical Correlation of Surficial Sediment from Area Drainages with Selected Sedimentary Interbeds at the Idaho National Engineering Laboratory, Idaho*, Water-Resources Investigations Report 90-4147, DOE/ID-22092, U.S. Geological Survey.

Bartholomay, R. C., L. L. Knobel, and L. C. Davis, 1989, *Mineralogy and Grain Size of Surficial Sediment from the Big List River Drainage and Vicinity, with Chemical and Physical Characteristics of Geologic Materials from Selected Sites at the Idaho National Engineering Laboratory, Idaho*, Open-File Report 89-384, DOE/ID-22081, U.S. Geological Survey, July 1989.

Bertetti, F. P., R. T. Pabalan, and M. G. Almendarez, 1998, "Studies of Neptunium(V) Sorption on Quartz, Clinoptilolite, Montmorillonite, and Alpha-Alumina," in: Adsorption of Metals by Geomedia, E. A. Jenne (ed), Academic Press, 132-149.

Breiman, L., J. H. Friedman, R. A. Olshen, and C. J. Stone, 1984, "Classification and Regression Trees," Wadsworth International Group.

Brunauer, S., P. H. Emmett, and E. Teller, 1938, "Adsorption of Gases in Multimolecular Layers," *Journal of the American Chemical Society*, Vol. 60, 309-319.

Case, M. J., A. S. Rood, J. M. McCarthy, S. O. Magnuson, and B. H. Becker, 2000, *Technical Revision of the Radioactive Waste Management Complex Low-Level Waste Radiological Performance Assessment for Calendar Year 2000*, INEEL/EXT-2000-01089.

Chisholm-Brause, C. J., J. M. Berg, R. A. Matzner, and D. E. Morris, 2001, "Uranium(VI) Sorption Complexes on Montmorillonite as a Function of Solution Chemistry," *Journal of Colloid and Interface Science*, Vol. 233 (1), 38-49.

Conover, W. J., 1980, "Practical Nonparametric Statistics, 2nd Ed.," Wiley, New York, NY.

Cressie, N. A. C., 1993, "Statistics for Spatial Data, Revised Edition," Wiley, New York, NY.

Davis, J. A., J. A. Coston, D. B. Kent, and C. C. Fuller, 1998, "Application of the Surface Complexation Concept to Complex Mineral Assemblages," *Environmental Science & Technology*, Vol. 32 (19), 2820-2828.

Davis, J. A. and D. B. Kent, 1990, "Surface Complexation Modeling in Aqueous Geochemistry," *Reviews in Mineralogy*, Vol. 23, 177-260.

EPA, 1999, *Understanding Variation in Partition Coefficient, Kd, Values*, EPA 402-R-99-004A, U.S. Environmental Protection Agency.

Fjeld, R. A., T. A. DeVol, R. W. Goff, M. D. Blevins, D. D. Brown, S. M. Ince, and A. W. Elzerman, 2001, "Characterization of the Mobilities of Selected Actinides and Fission/Activation Products in Laboratory Columns Containing Subsurface Material from the Snake River Plain," *Nuclear Technology*, Vol. 135 (2), 92-108.

Gilbert, R. O., 1987, "Statistical Methods for Environmental Pollution Monitoring," Van Nostrand Reinhold Company.

Grossman, C. J., R. A. Fjeld, J. T. Coates, and A. W. Elzerman, 2001, *The Sorption of Selected Radionuclides in Sedimentary Interbed Soils from the Snake River Plain*, INEEL/EXT-01-01106, Clemson University, Department of Environmental Engineering and Science, June 2001.

Holdren, K. J., B. H. Becker, L. D. Koeppen, S. O. Magnuson, T. J. Meyer, G. L. Olson, and A. J. Sondrup, 2002, *Ancillary Basis for Risk Analysis of the Subsurface Disposal Area*, INEEL/EXT-02-01125, September 2002.

Hull, L. C., C. Grossman, R. A. Fjeld, J. T. Coates, and A. W. Elzerman, 2003, "Hybrid Empirical - Theoretical Approach to Modeling Uranium Adsorption," *Applied Geochemistry*, (accepted for publication).

Jackson, M. L., C. H. Lim, and L. W. Zelazny, 1986, "Oxides, Hydroxides, and Aluminosilicates," in: Methods of Soil Analysis Part 1. Physical and Mineralogical Methods, A. Klute (ed), 9, American Society of Agronomy and Soil Science Society of America, 101-150.

Kaplan, D. I. and R. J. Serne, 1995, "Distribution Coefficient Values Describing Iodine, Neptunium, Selenium, Technetium, and Uranium Sorption to Hanford Sediments," PNL-10379, Sup 1, Pacific Northwest National Laboratory.

Kaplan, D. I., R. J. Serne, and M. G. Piepho, 1995, "Geochemical Factors Affecting Radionuclide Transport through near and Far Fields at a Low-Level Waste Disposal Site," PNL-10379, Pacific Northwest National Laboratory.

Koch, G. S., Jr. and R. F. Link, 1980, *Statistical Analyses of Geological Data, vols I. II.*, Dover, New York.

Kohler, M., B. D. Honeyman, and J. O. Leckie, 1999, "Neptunium(V) Sorption on Hematite (Alpha-Fe_2O_3) in Aqueous Suspension: The Effect of CO_2," *Radiochimica Acta*, Vol. 85 (1), 33-48.

Leecaster, M. K., 2002, *Geostatistic Modeling of Subsurface Characteristics in the Radioactive Waste Management Complex Region, Operable Unit 7-13/14*, INEEL/EXT-02-00029, May 2002.

MacIntyre, W. G., C. P. Antworth, T. B. Stauffer, and R. G. Young, 1998, "Heterogeneity of Sorption and Transport-Related Properties in a Sand-Gravel Aquifer at Columbus, Mississippi," *Journal of Contaminant Hydrology*, Vol. 31 (3-4), 257-274.

Magnuson, S. O. and A. J. Sondrup, 1998, *Development, Calibration, and Predictive Results of a Simulator for Subsurface Pathway Fate and Transport of Aqueous and Gaseous-Phase Contaminants in the Subsurface Disposal Area at the Idaho National Engineering and Environmental Laboratory*, INEEL/EXT-97-00609, July 1998.

Mattigod, S. V. and W.J. Martin, 2001, *Radionuclide Activities in Contaminated Soils: Effects of Sampling Bias on Remediation of Coarse-Grained Soils in Hanford Formation*, PNNL-13624, August 2001.

McCarthy, J. M., B. H. Becker, S. O. Magnuson, K. N. Keck, and T. K. Honeycutt, 2000, *Radioactive Waste Management Complex Low-Level Waste Radiological Composite Analysis*, INEEL/EXT-97-01113.

McKinley, J. P., J. M. Zachara, S. C. Smith, and G. D. Turner, 1995, "The Influence of Uranyl Hydrolysis and Multiple Site-Binding Reactions on Adsorption of U(VI) to Montmorillonite," *Clays and Clay Minerals*, Vol. 43 (5), 586-598.

Newman, M. E., I. Porro, R. Scott, and F. M. Dunnivant, 1996, *Evaluation of the Mobility of Am, Cs, Co, Pu, Sr, and U through INEL Basalt and Interbed Materials: Summary Report of the INEL/Clemson University Laboratory Studies*, INEL-95/282.

Painter, S., V. Cvetkovic and D. R. Turner, 2001, "Effect of Heterogeneity on Radionuclide Retardation in the Alluvial Aquifer near Yucca Mountain, Nevada," *Journal of Ground Water*, Vol. 39 (3), 326-338.

Rhoades, J. D., 1982, "Cation Exchange Capacity," in: Methods of Soil Analysis Part 2 Chemical and Microbiological Properties, A. L. Page, R. H. Miller, and D. R. Keeney (ed), 9, American Society of Agronomy and Soil Science Society of America, 149-158.

Rightmire, C. T. and B. D. Lewis, 1987, *Hydrology and Geochemistry of the Unsaturated Zone, Radioactive Waste Management Complex, Idaho National Engineering Laboratory, Idaho*, Water-Resources Investigations Report 87-4198, DOE/ID-22073, U.S. Geological Survey, November 1987.

Ripley, B. D., 1981, "Spatial Statistics", Wiley, New York, NY.

Roback, R. C., D. W. Efurd, M. T. Murrell, R. E. Steiner, and C. J. Duffy, 2000, "Assessment of Uranium and Plutonium in the Saturated and Unsaturated Zones beneath the Subsurface Disposal Area, INEEL," LA-UR-00-5471, Los Alamos National Laboratory.

Robin, M. J. L., E. A. Sudicky, R. W. Gillham, and R. G. Kachanoski, 1991, "Spatial Variability of Strontium Distribution Coefficients and Their Correlation with Hydraulic Conductivity in the Canadian Forces Base Borden Aquifer," *Water Resources Research*, Vol. 27 (10), 2619-2632.

Shapiro, S. S. and M. B. Wilk, 1965, "An Analysis of Variance Test for Normality (Complete Samples)," *Biometrika*, Vol. 52, 591-611.

Snedecor, G. W. and W. G. Cochran, 1980, "Statistical Methods, 7th Ed.," Iowa State University Press.

Stein, M. L., 1988, "Asymptotically Efficient Prediction of a Random Field with a Misspecified Covariance Function," *Annals of Statistics*, Vol. 16 (1), 55-63.

Sylwester, E. R., E. A. Hudson, and P. G. Allen, 2000, "The Structure of Uranium (VI) Sorption Complexes on Silica, Alumina, and Montmorillonite," *Geochimica Et Cosmochimica Acta*, Vol. 64 (14), 2431-2438.

Turner, D. R., 1995, "A Uniform Approach to Surface Complexation Modeling of Radionuclide Sorption," CNWRA 95-001, Center for Nuclear Waste Regulatory Analysis.

Turner, D. R. and R. T. Pabalan, 1999, "Abstraction of Mechanistic Sorption Model Results for Performance Assessment Calculations at Yucca Mountain, Nevada," *Waste Management*, Vol. 19 (6), 375-388.

Viswanathan, H. S., B. A. Robinson, C. W. Gable, and J. W. Carey, 2003, "A Geostatistical Modeling Study of the Effect of Heterogeneity on Radionuclide Transport in the Unsaturated Zone, Yucca Mountain," *Journal of Contaminant Hydrology*, Vol. 62 (3), 319-336.

Waite, T. D., J. A. Davis, T. E. Payne, G. A. Waychunas, and N. Xu, 1994, "Uranium(VI) Adsorption to Ferrihydrite - Application of a Surface Complexation Model," *Geochimica Et Cosmochimica Acta*, Vol. 58 (24), 5465-5478.

Whittig, L. D. and W. R. Allardice, 1986, "X-Ray Diffraction Techniques," in: Methods of Soil Analysis Part 1. Physical and Mineralogical Methods, A. Klute (ed), 9, American Society of Agronomy and Soil Science Society of America, 331-362.